「円盤銀河の形成と進化研究会」 2013.9.26-28

円盤銀河形成進化シナリオと問題点

梅村　雅之

筑波大学　計算科学研究センター

Contents

- ❖ 銀河形成の物理
  - 銀河形成の三種の神器
  - 散逸銀河形成／非散逸銀河形成
  - UV/SN フィードバック
- ❖ 銀河形成シミュレーションと問題点
  - 質量問題
  - 角運動量問題
  - Substructure 問題

鏡　CDM Density Fluctuations
銀河の大域的分布

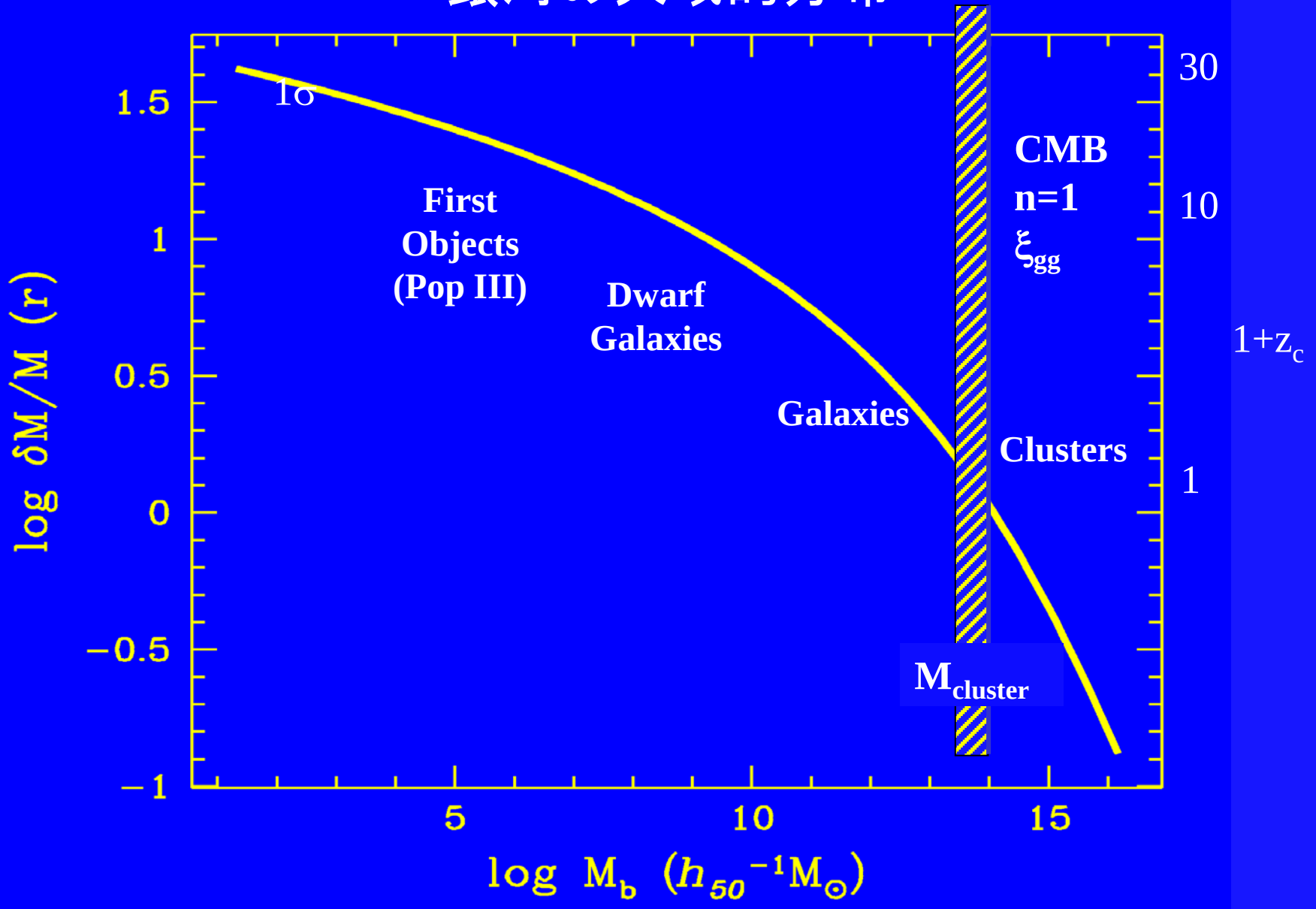

剣　Random Gaussian Density Fields

(Bardeen et al. 1986)

Peak statistics　ξ(ν大)> ξ(ν小)

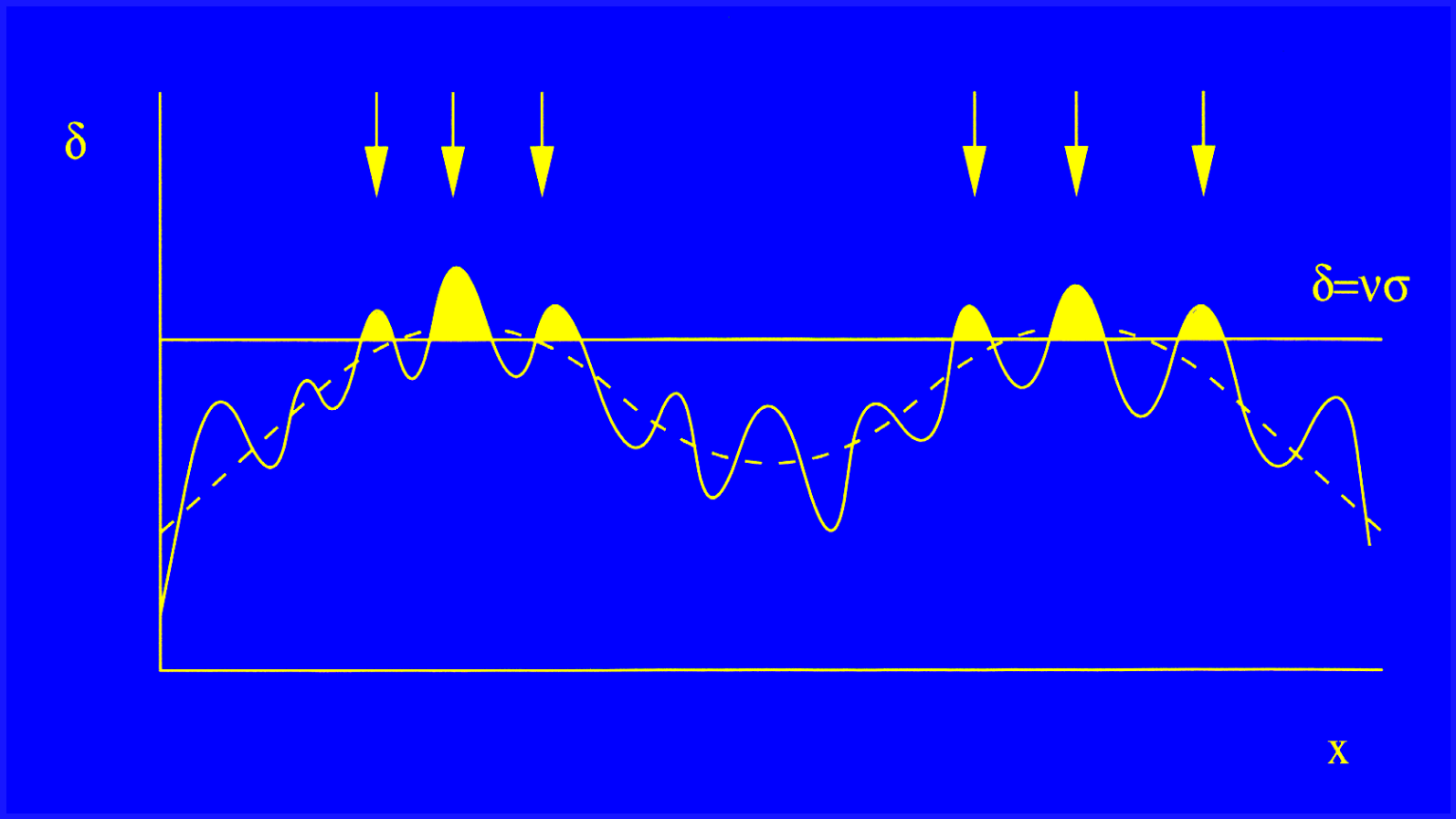

Gravitational Instability

Jeans Criterion（Gravitational energy>internal energy）

$$M > M_J = \left(\frac{kT}{G}\right)^{3/2} m_p^{-2} n^{-1/2}$$

(k: Boltzmann constant, m_p: proton mass,

T: temperature, n: numberdensity)

Cooling Process

- **Present-day**
  metal cooling, dust cooling

- **First stars, First galaxies**
  H_2 molecule cooling

玉 Cooling Diagram

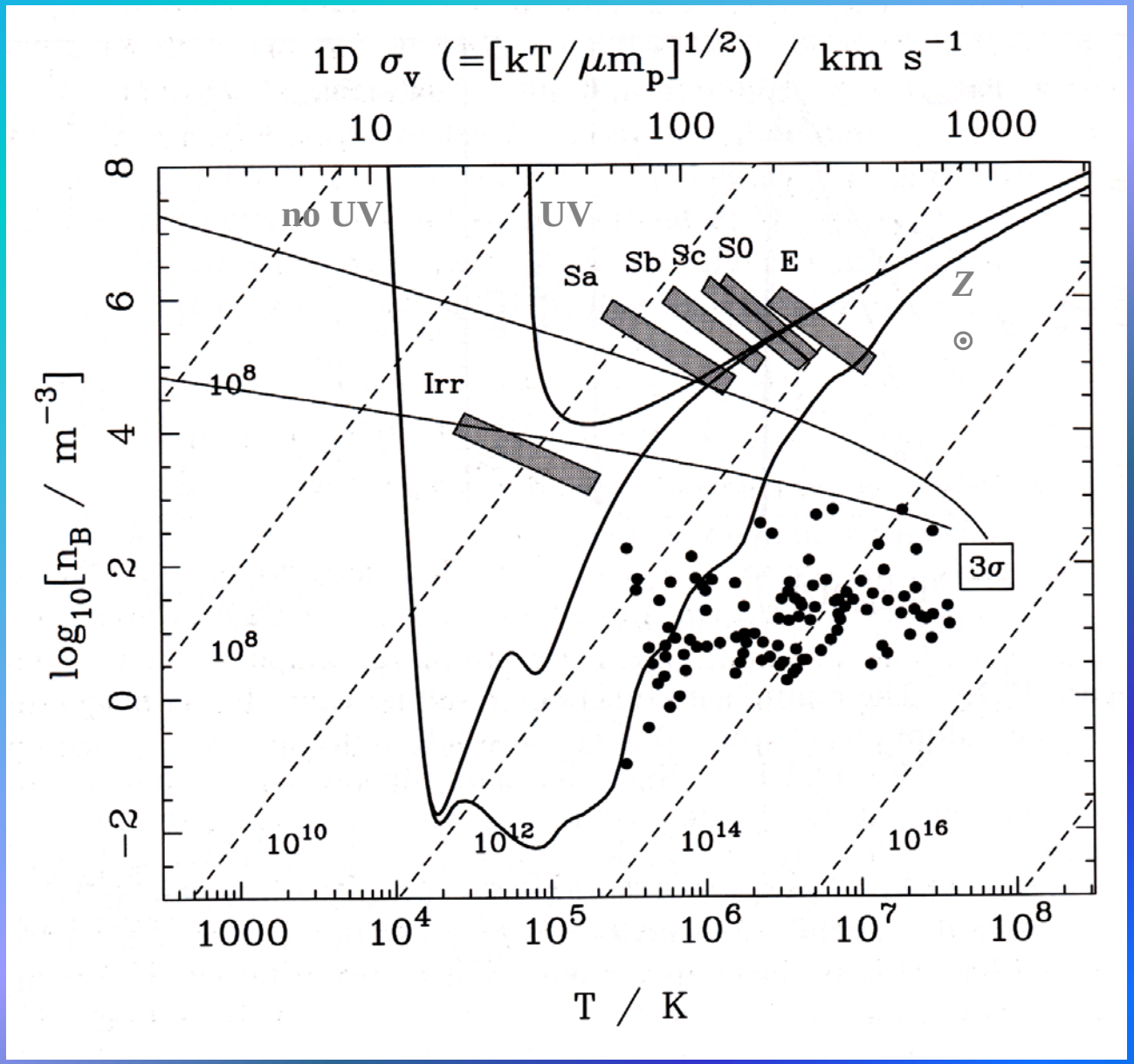

Rees & Ostriker 1977; Blumenthal et al. 1984

$$M \le \alpha^5 \left(\frac{M_p}{m_p}\right)^4 \left(\frac{m_p}{m_e}\right)^{1/2} m_p$$

$$\approx 10^{11} M_\odot$$

Three Elements for Galaxy Formation

CDM Fluctuations

Random Gaussian Density Fields

Cooling Diagram (Rees & Ostriker 1977)

+

c_* -prescription for star formation

$$\frac{d\rho_*}{dt} = c_* \frac{\rho_{gas}}{t_{ff}}$$

銀河形態の起源

- **Monolithic collapse**

  (Eggen, Lynden-Bell & Sandage 1962; Partridge & Peebles 1967; Larson 1974)

  Larson's paradigm (morphological bifurcation)

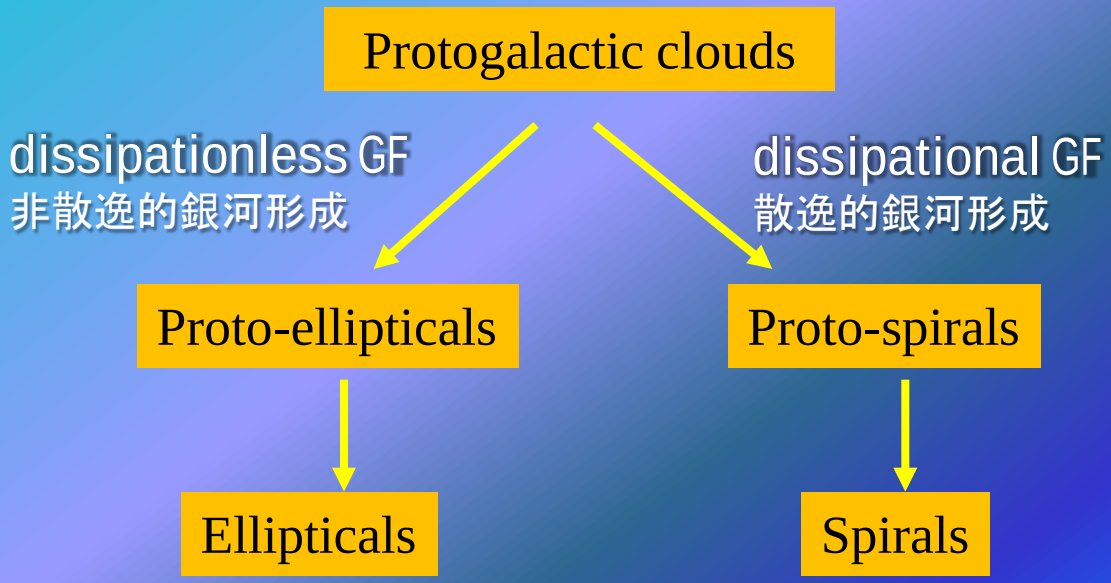

- **Merger hypothesis**

  (White & Rees 1978; Frenk et al. 1985)

  Disk major merger → Ellipticals

  N-body, Hydro-simulation, Semi-analytic

Dissipationless/Dissipational Galaxy Formation Paradigm

(Larson 1969, 1974, 1975, 1976)

$$\frac{\partial f}{\partial t} + \mathbf{v}\frac{\partial f}{\partial \mathbf{r}} + \mathbf{a}\frac{\partial f}{\partial \mathbf{v}} = \left(\frac{\partial f}{\partial t}\right)^{*} \qquad \frac{d\rho_s}{dt} = C\rho_g{}^{n}$$

High Star Formation Rate (SFR) → Elliptical Galaxies
Low Star Formation Rate → Spiral Galaxies

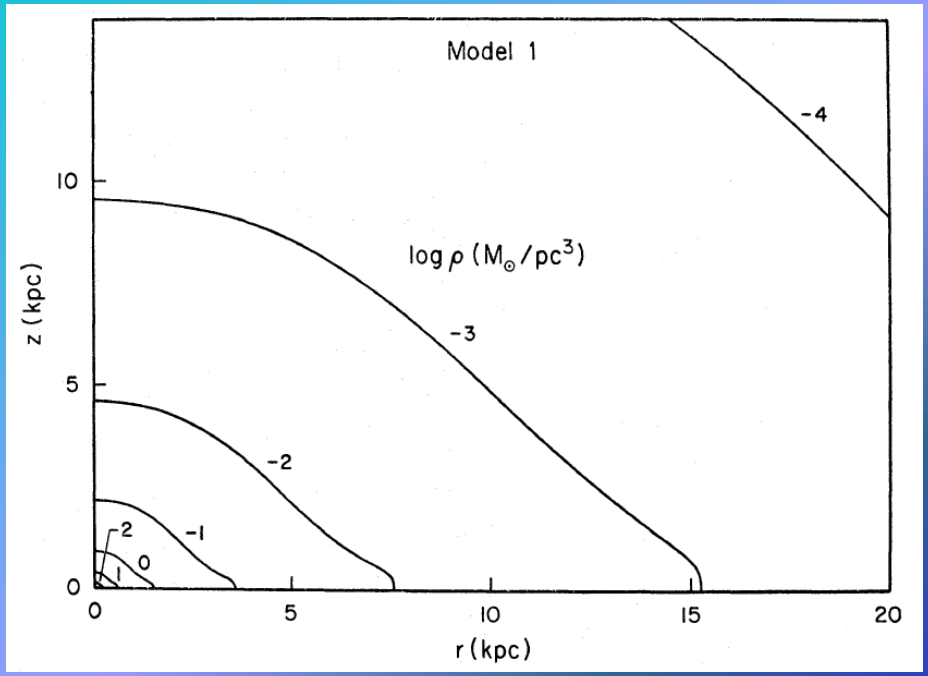

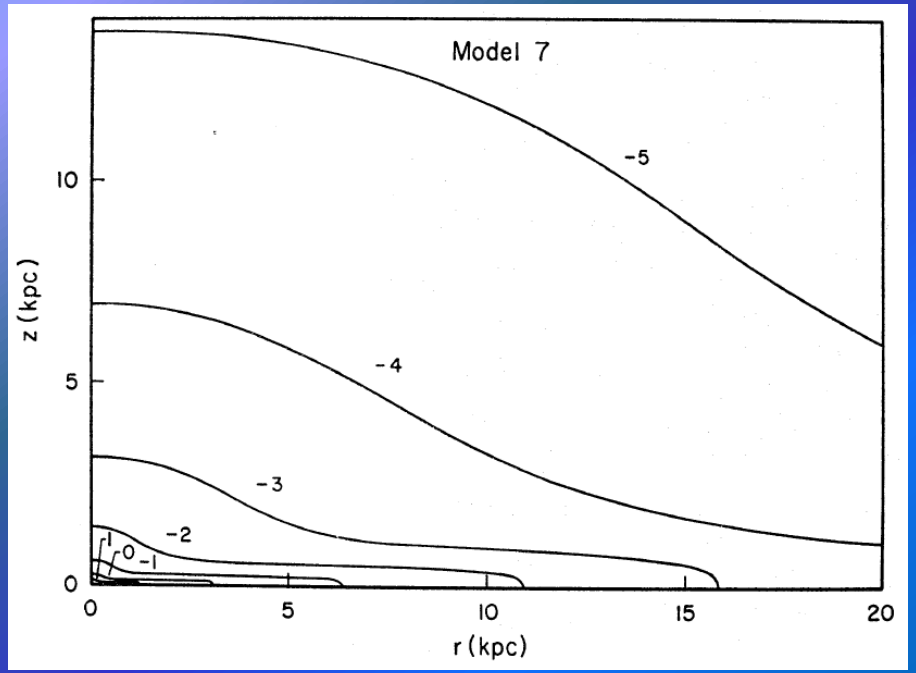

非散逸的銀河形成（左）と散逸的銀河形成（右）のシミュレーション。2次元r-z平面での密度分布の輪郭を表す。非散逸的銀河形成では密度分布は楕円体となり，散逸的銀河形成では楕円体成分と円盤成分が形成される。（Larson, R. B. 1976, Mon. Not. Roy. Astron. Soc., **176**, 31 より転載）

GF Simulations with Star Formation (SPH)

Star Formation Criteria

1. div **v** < 0
2. Jeans unstable
3. $T < T_c (\approx \text{a few} \times 10^4 K)$
4. $n > n_c (\approx 0.01\ \text{cm}^{-3})$

$$\rightarrow \quad \frac{d\rho_*}{dt} = -\frac{d\rho_g}{dt} = \frac{c_* \rho_g}{t_{ff}}$$

$$p_* = 1 - \exp\left[-\frac{c_* \Delta t}{t_{ff}}\right]$$

Disk Galaxy

$c_* = 0.05$

Steinmetz & Navarro (1999)
Navarro & Steinmetz (2000)
Koda et al. (2000)

Elliptical Galaxy, Bulge

$c_* = 1$

Kawata (1999)

δ=νσ と SFR(c_*) の関係は？

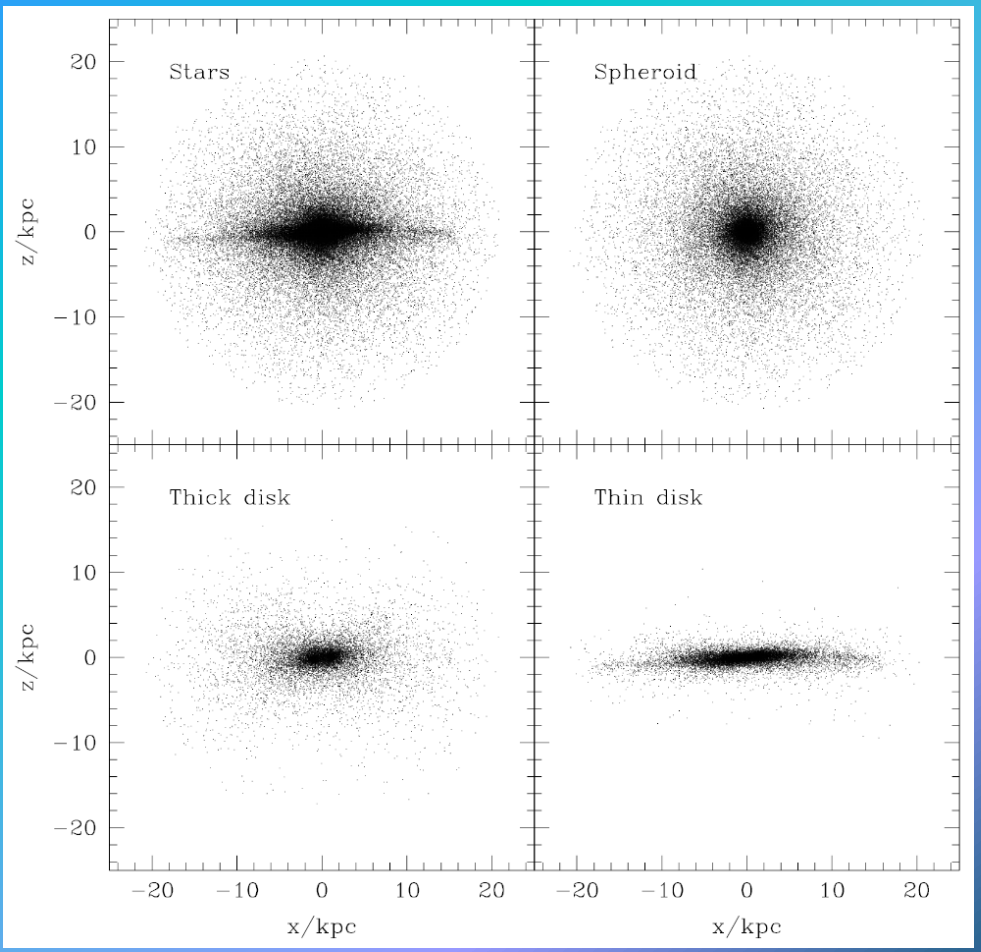

Abadi, Metal. 2003

左上は全ての星成分，右上は球状の古い星成分，左下は厚い円盤成分，右下は薄い円盤成分を表す。

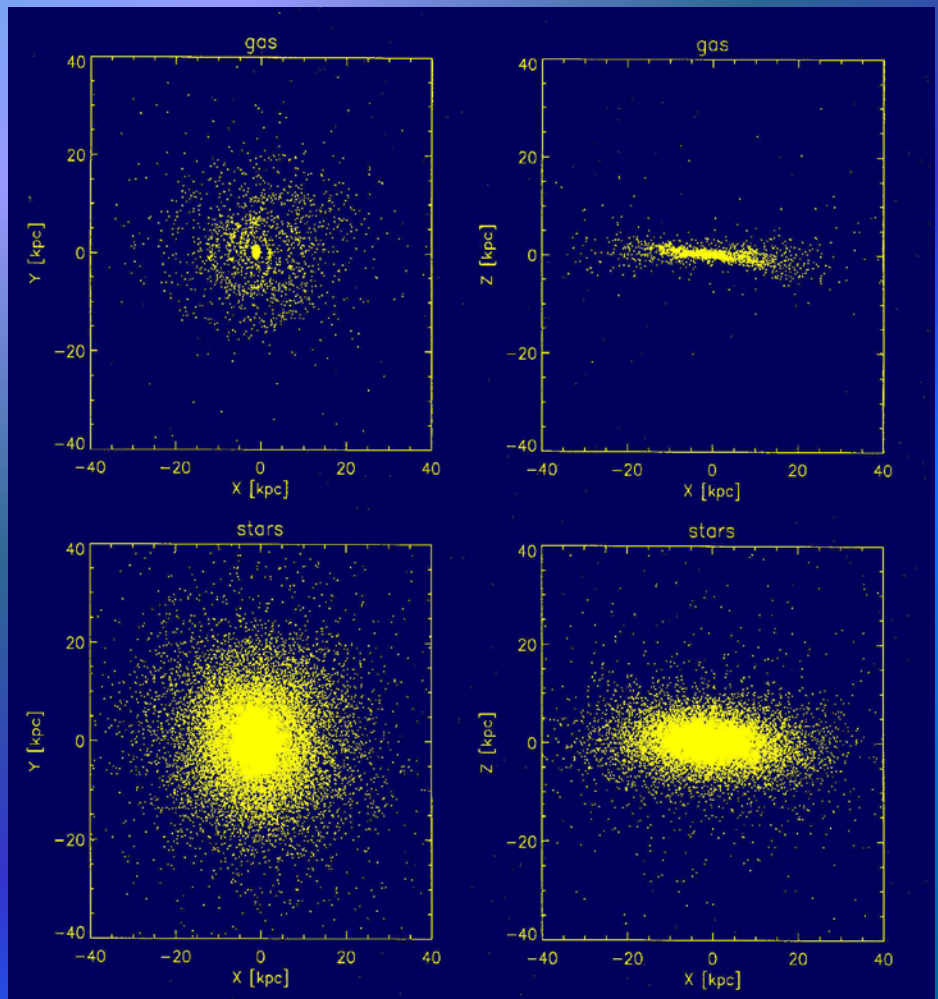

Steinmetz & Muller 1995

Disk Merger Hypothesis

GC3 - Grand Challenge Cosmology Consortium-
Cluster Simulations on the PSC Cray T3E

John Dubinski 2003

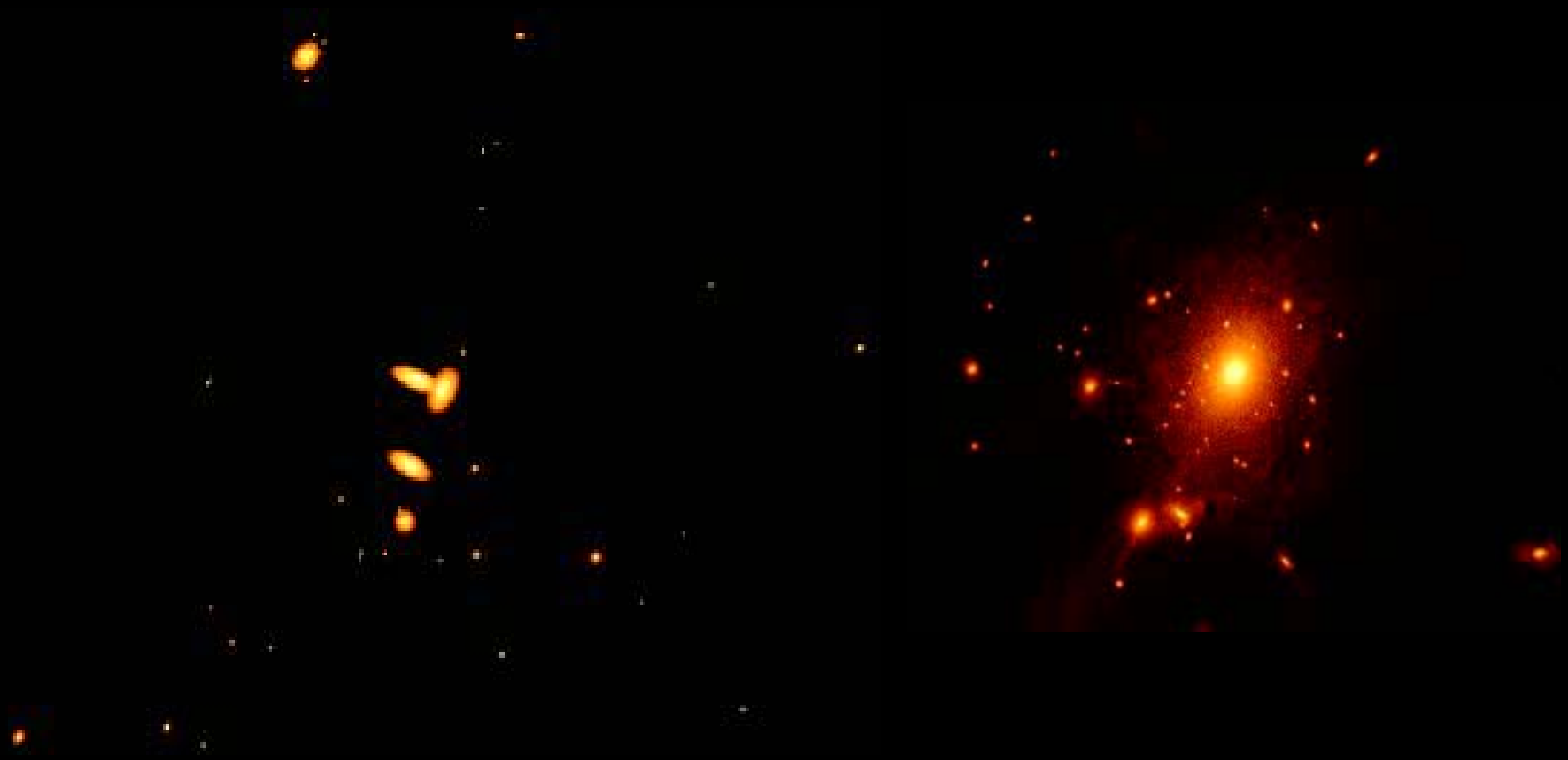

Ostriker's Objection to Disk Merger Hypothesis

Elliptical Galaxies are not Made by Merging Spiral Galaxies
Ostriker, J.P. 1980, Comments on Astrophysics 8, 177

1. **Relative velocities between the interacting galaxies are too high to allow a merger in the centers of rich clusters where the highest concentrations of ellipticals are seen.**

2. **Ellipticals display color-luminosity and metallicity-luminosity correlations that argue aganist an origin in the stochastic aggregation of similar subunits.**

3. **Ellipticals and bulges in spirals have several common properties, which might imply a common origin.**

4. **The central phase space density in ellipticals is significantly higher than that in spirals. This quantity should be conserved in a merger.**

5. **The specific frequency of globular clusters in ellipticals is higher than that in spirals.**

Phase Space Density Problem

Carlberg, 1986
ApJ, 310, 593

$$f_c = \frac{9}{2(2\pi)^{5/2}} \frac{1}{\sigma_c r_c^2}$$

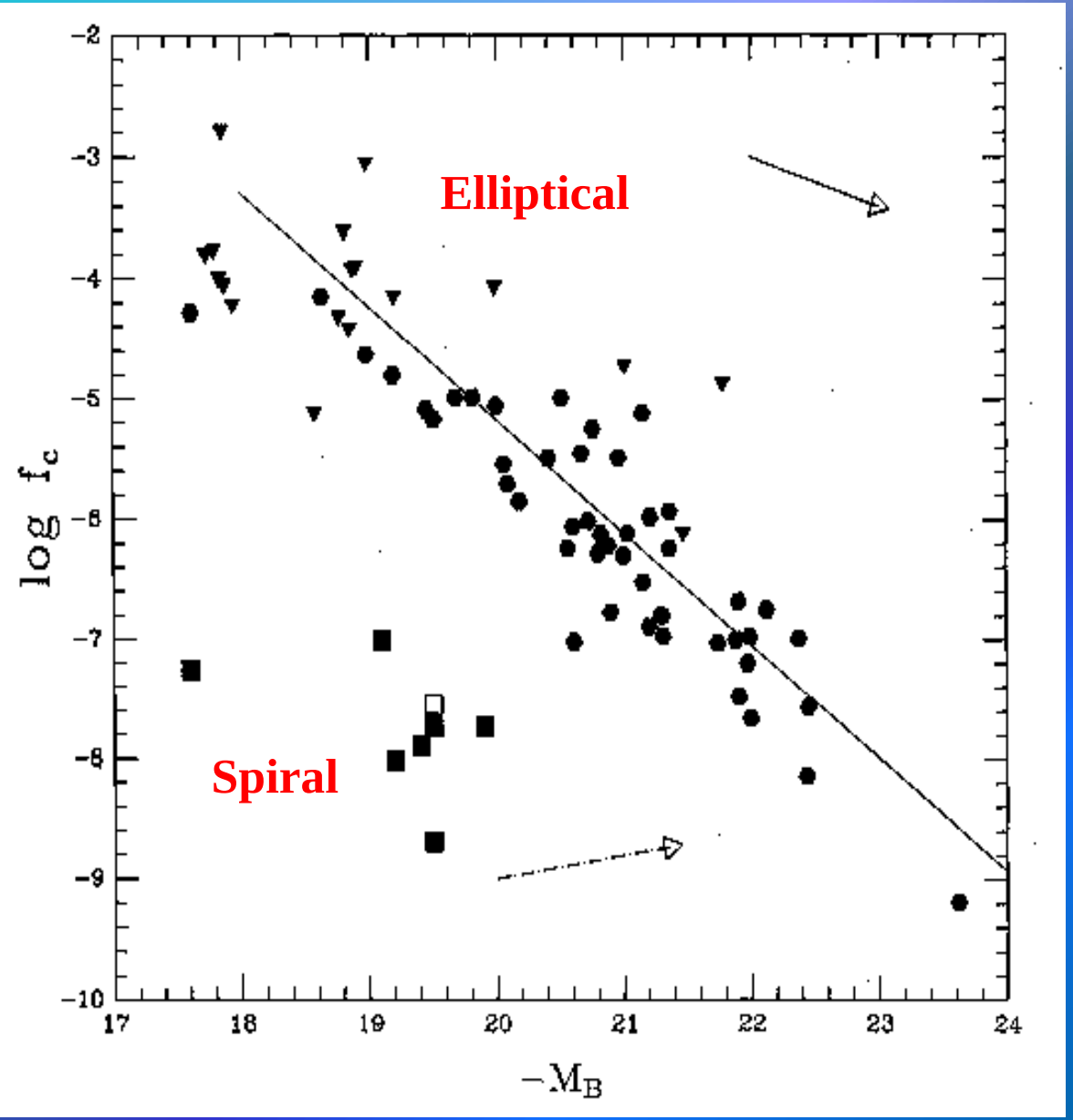

CDM Density Fluctuations

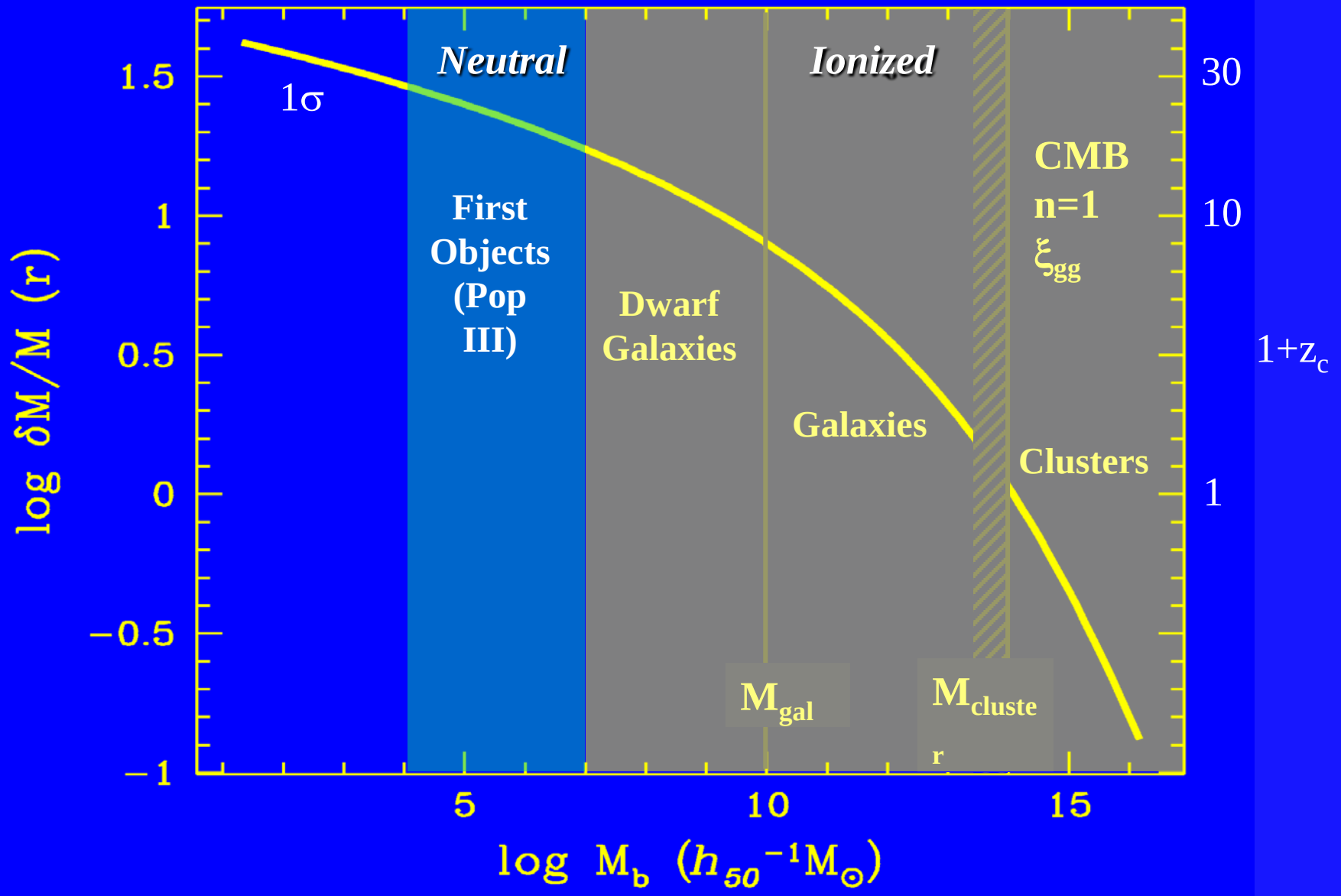

Three Elements for Galaxy Formation

CDM Fluctuations

Random Gaussian Density Fields

Cooling Diagram (Rees & Ostriker 1977)

+

Self-Shielding

紫外線背景放射から自己遮蔽されなければ，星は形成されない!!

No stars form unless baryonic matter is self-shielded from UVB !

Self-Shielding

Tajiri & MU, 1998, ApJ, 502, 59

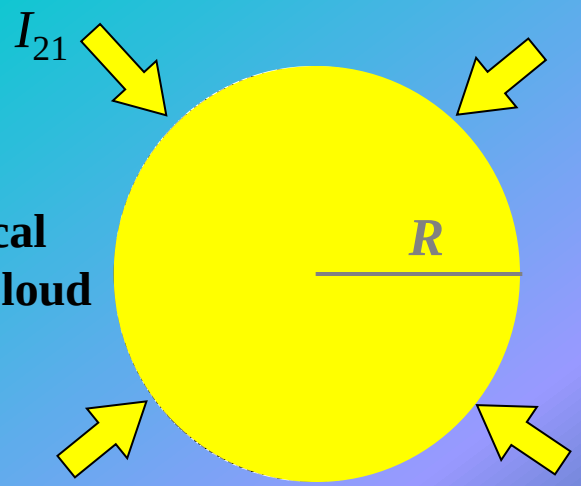

Spherical top-hat cloud

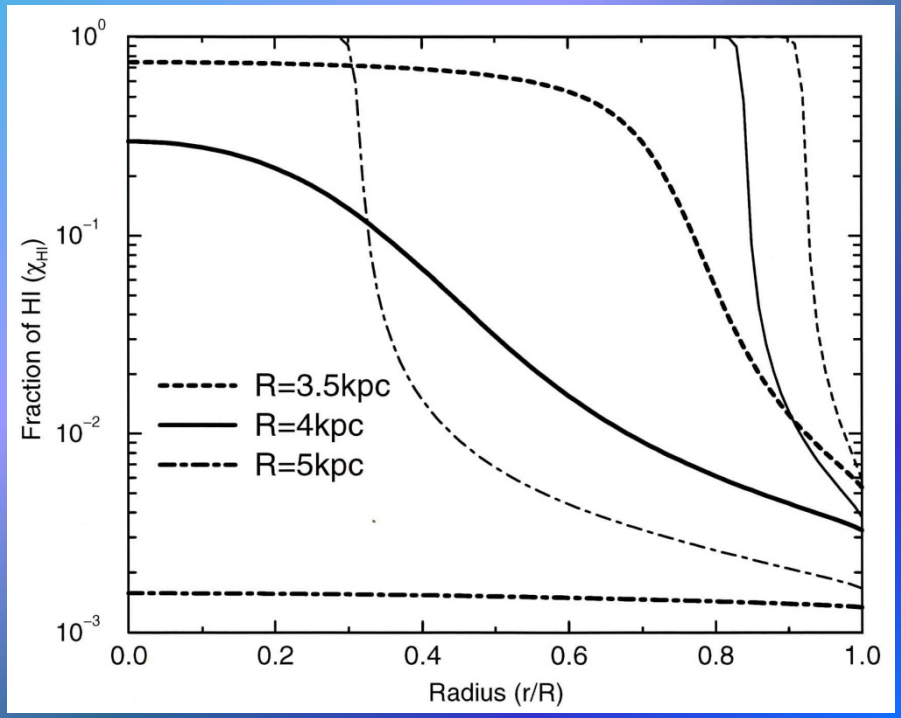

$$n_{crit} = 1.5\times10^{-2} M_8^{-1/5} (I_{21}/\alpha)^{3/5} \ \mathrm{cm}^{-3}$$

$$(M_8 = M/10^8 M_\odot, \quad T = 10^4 \mathrm{K})$$

$$\tau_{\mathrm{crit}} \equiv n_{\mathrm{HI}} a_{\nu_L} R_{\mathrm{crit}} = 0.6 \frac{\alpha+3}{\alpha}$$

Galaxy Formation in UV background

Susa & MU 2000, MNRAS, 316, L17

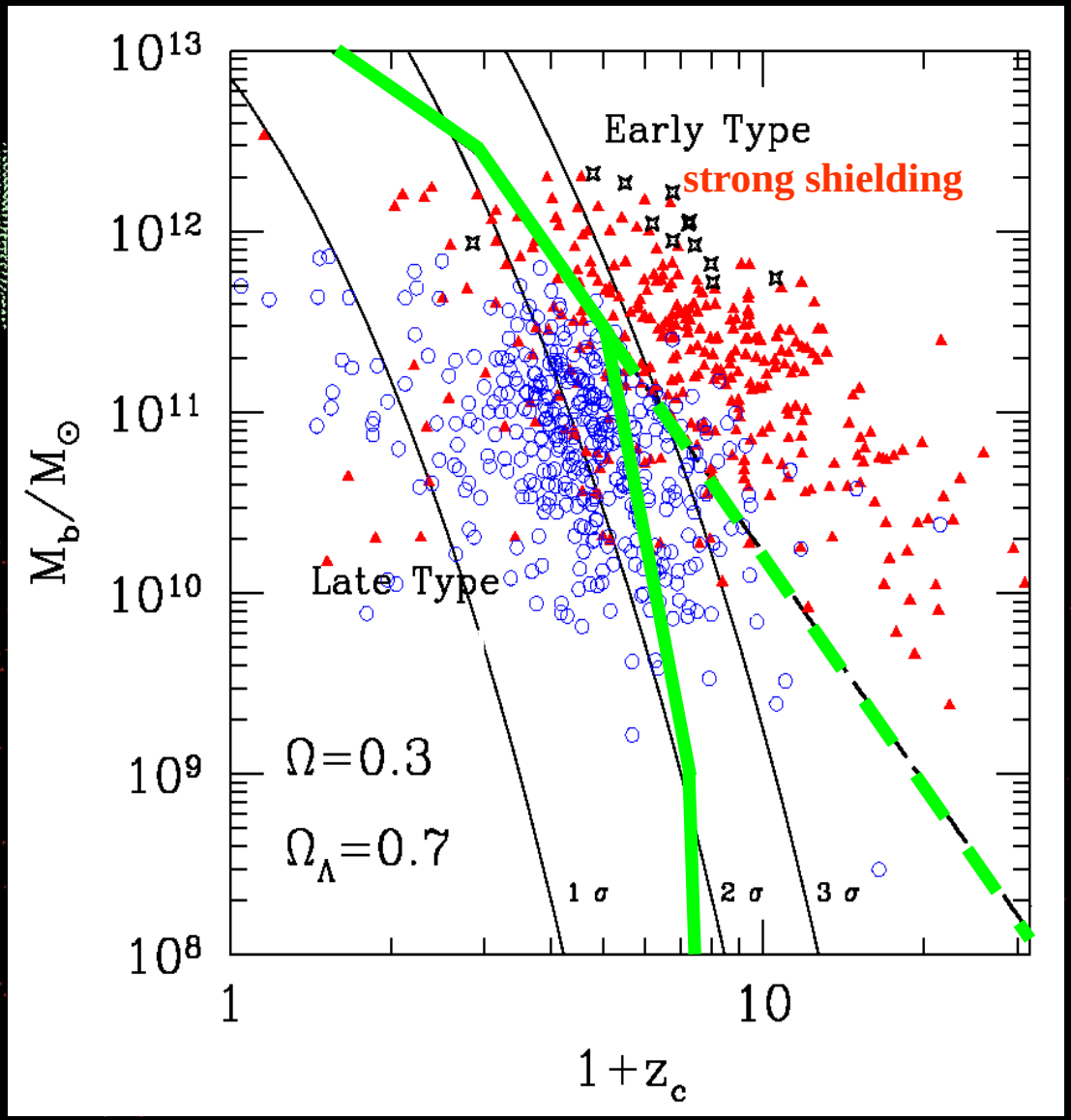

From Primeval Irregulars to Present-day Ellipticals

Mori and Umemura, 2006, Nature, 440, 644

Simulation (high-resolution)

z=3.1 LAE

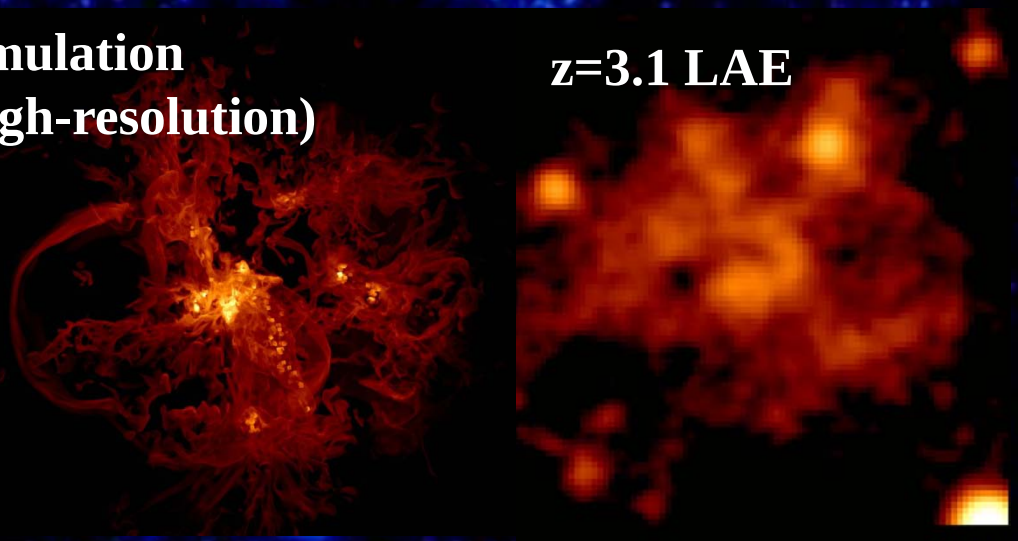

Total Mass: $10^{11}\ M_\odot$
Gas Mass: $1.3 \times 10^{10}\ M_\odot$
# of Subunits: 20
Box Size: 134 kpc
Grid Points: 1024^3

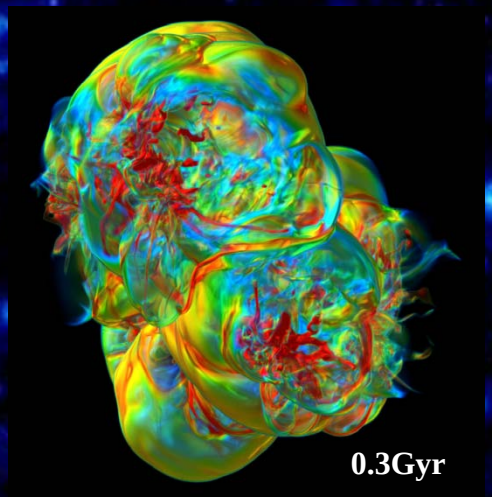

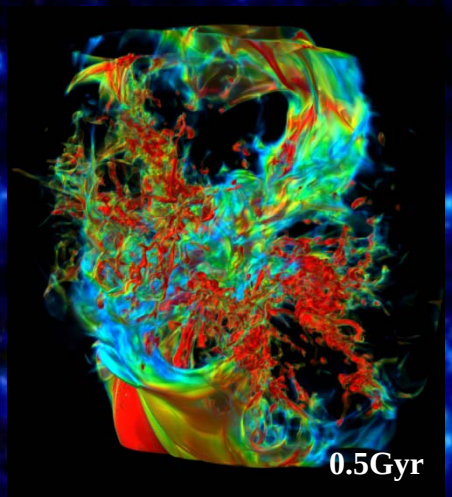

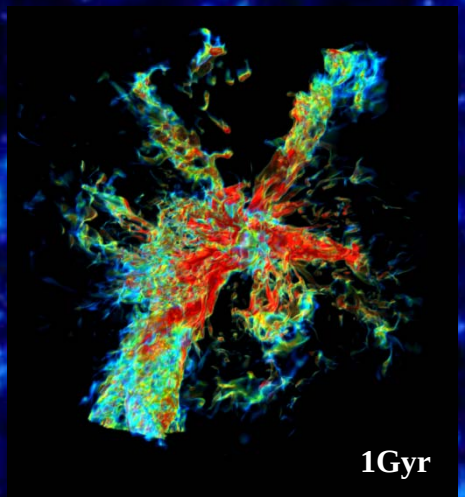

Lyman α Emitters (LAE) Evolves into Elliptical Galaxies

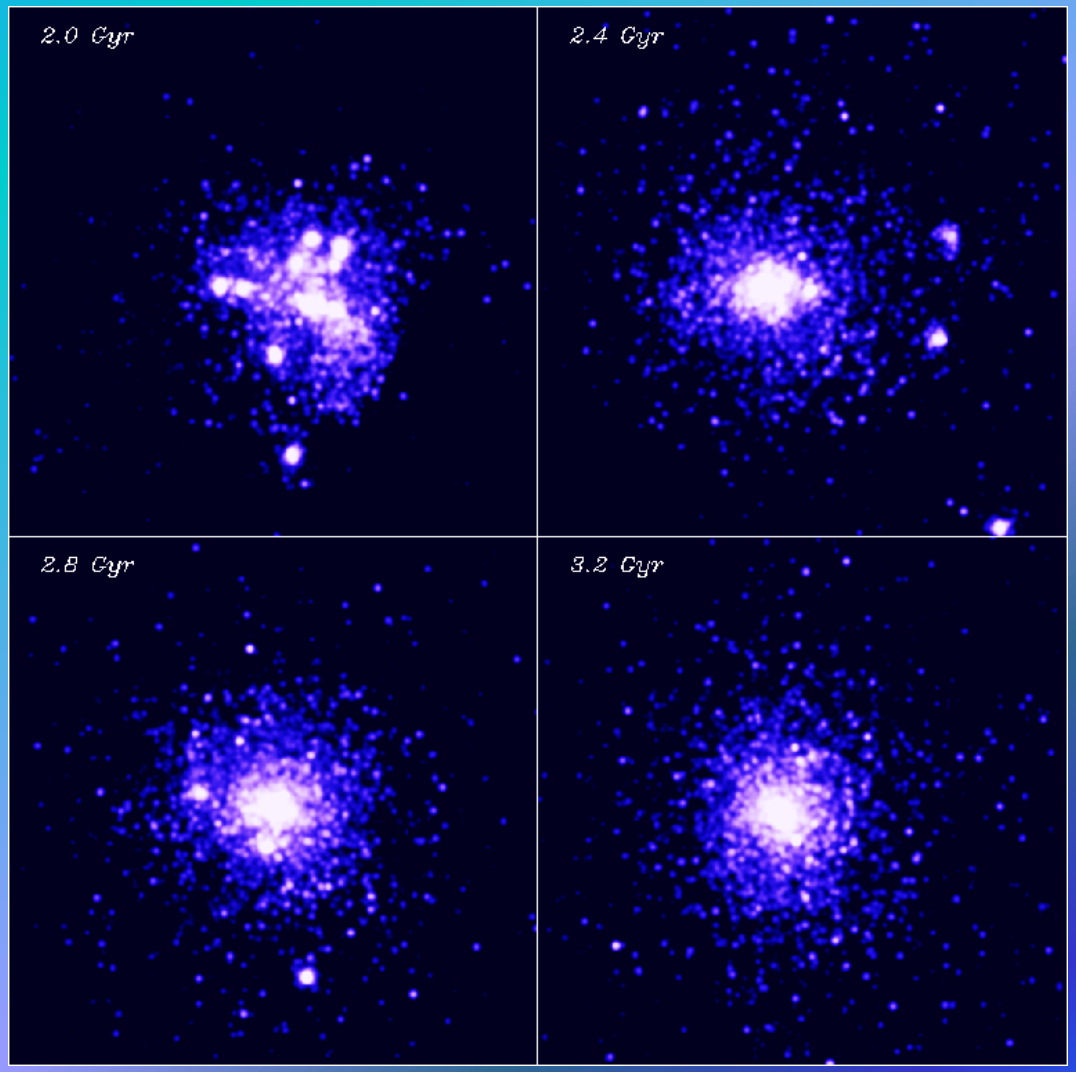

The virializaion of the total system is almost completed 3 Gyrs.

The resultant system at 13 Gyrs (redshift z=0) :

Stellar mass: $M_{*}=1.1\times10^{10}\ M_{\odot}$

Central velocity dispersion: V_0=133 km s^{-1}

Effective radius: R_e=3.97 kpc

B-band mag.: M_B= -17.2

V-band mag.: M_V= -18.0

Color: *U*-*V*=1.15

V-*K*=2.85

These values are consistent with the properties of the present-day less-massive elliptical galaxies.

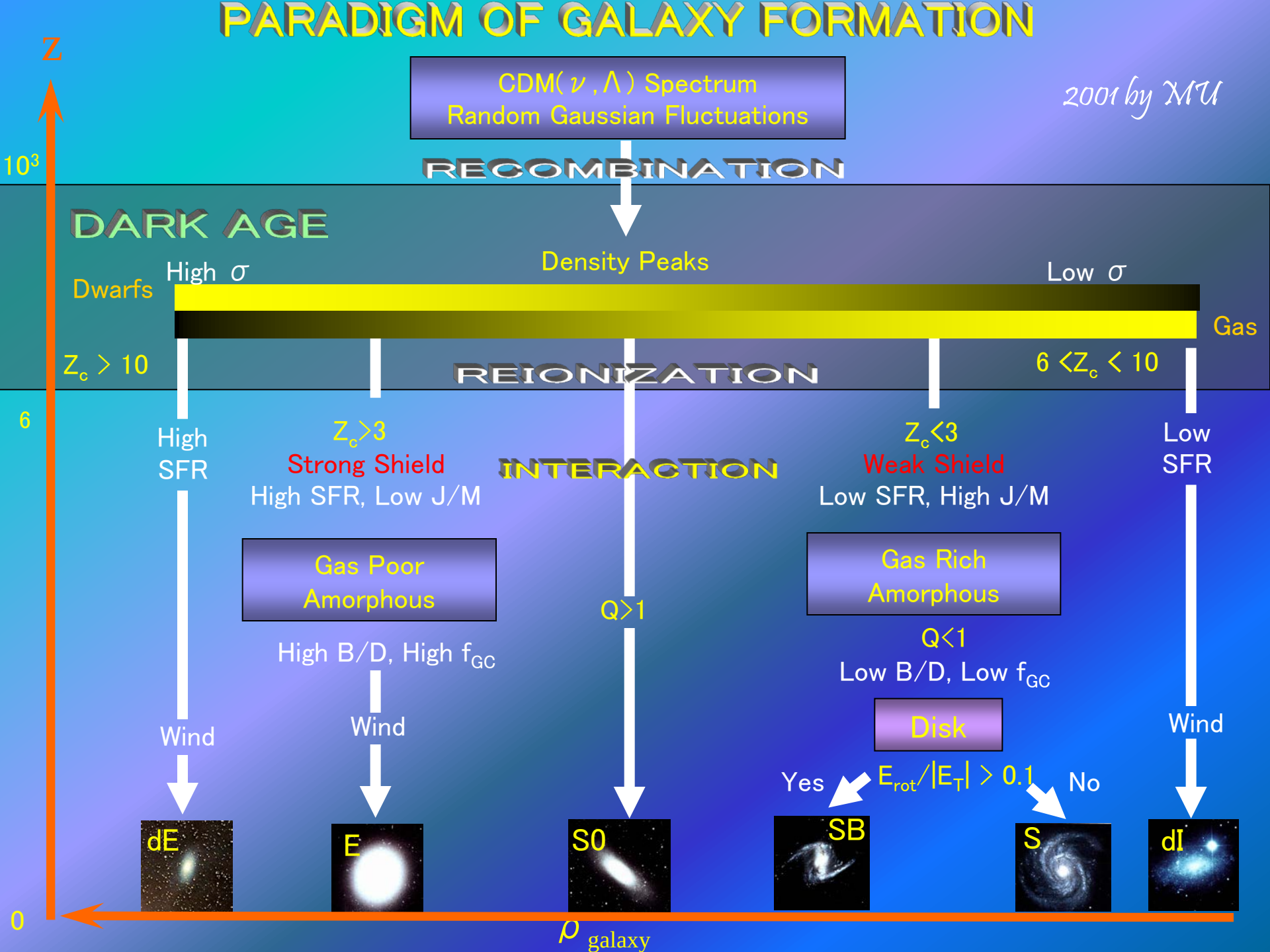
PARADIGM OF GALAXY FORMATION
2001 by MU
z
10^3
CDM(ν , Λ) Spectrum
Random Gaussian Fluctuations
RECOMBINATION
DARK AGE
Density Peaks
High σ
Low σ
Dwarfs
Gas
$Z_c > 10$
$6 < Z_c < 10$
REIONIZATION
6
High SFR
$Z_c > 3$
Strong Shield
High SFR, Low J/M
INTERACTION
$Z_c < 3$
Weak Shield
Low SFR, High J/M
Low SFR
Gas Poor
Amorphous
Gas Rich
Amorphous
Q>1
Q<1
High B/D, High f_{GC}
Low B/D, Low f_{GC}
Disk
Wind
Wind
Wind
Yes
$E_{rot}/|E_T| > 0.1$
No
dE
E
S0
SB
S
dI
0
ρ_{galaxy}

宇宙論的銀河形成シミュレーション

❖ 銀河形態起源

1) Primordial Ellipticals (Bulges)

2) Primordial Disks

❖ 銀河形成シミュレーションの問題

1)質量問題

2)角運動量問題

The Aquila comparison project

Scannapieco et al., 2012, MNRAS, 423, 1726

Table 1. Summary of code characteristics and subgrid physics.

Code	Reference	Type	UV background (z_{UV})	UV background (spectrum)	Cooling	Feedback
G3 (GADGET3)	[1]	SPH	6	[10]	Primordial [13]	SN (thermal)
G3-BH	[1]	SPH	6	[10]	Primordial [13]	SN (thermal), BH
G3-CR	[1]	SPH	6	[10]	Primordial [13]	SN (thermal), BH, CR
G3-CS	[2]	SPH	6	[10]	Metal dependent [14]	SN (thermal)
G3-TO	[3]	SPH	9	[11]	Element-by-element [15]	SN (thermal+kinetic)
G3-GIMIC	[4]	SPH	9	[11]	Element-by-element [15]	SN (kinetic)
G3-MM	[5]	SPH	6	[10]	Primordial [13]	SN (thermal)
G3-CK	[6]	SPH	6	[10]	Metal dependent [14]	SN (thermal)
GAS (GASOLINE)	[7]	SPH	10	[12]	Metal dependent [16]	SN (thermal)
R (RAMSES)	[8]	AMR	12	[10]	Metal dependent [14]	SN (thermal)
R-LSFE	[8]	AMR	12	[10]	Metal dependent [14]	SN (thermal)
R-AGN	[8]	AMR	12	[10]	Metal dependent [14]	SN (thermal), BH
AREPO	[9]	Moving mesh	6	[10]	Primordial [13]	SN (thermal)

Note: [1] Springel et al. (2008); [2] Scannapieco et al. (2005), Scannapieco et al. (2006); [3] Okamoto et al. (2010); [4] Crain et al. (2009); [5] Murante et al. (2010); [6] Kobayashi, Springel & White (2007); [7] Stinson et al. (2006); [8] Teyssier (2002), Rasera & Teyssier (2006), Dubois & Teyssier (2008); [9] Springel (2010a); [10] Haardt & Madau (1996); [11] Haardt & Madau (2001); [12] Haardt & Madau (private communication); [13] Katz et al. (1996); [14] Sutherland & Dopita (1993); [15] Wiersma, Schaye & Smith (2009a); [16] Shen, Wadsley & Stinson (2010).

質量問題

The Aquila comparison project: the effects of feedback and numerical methods on simulations of galaxy formation

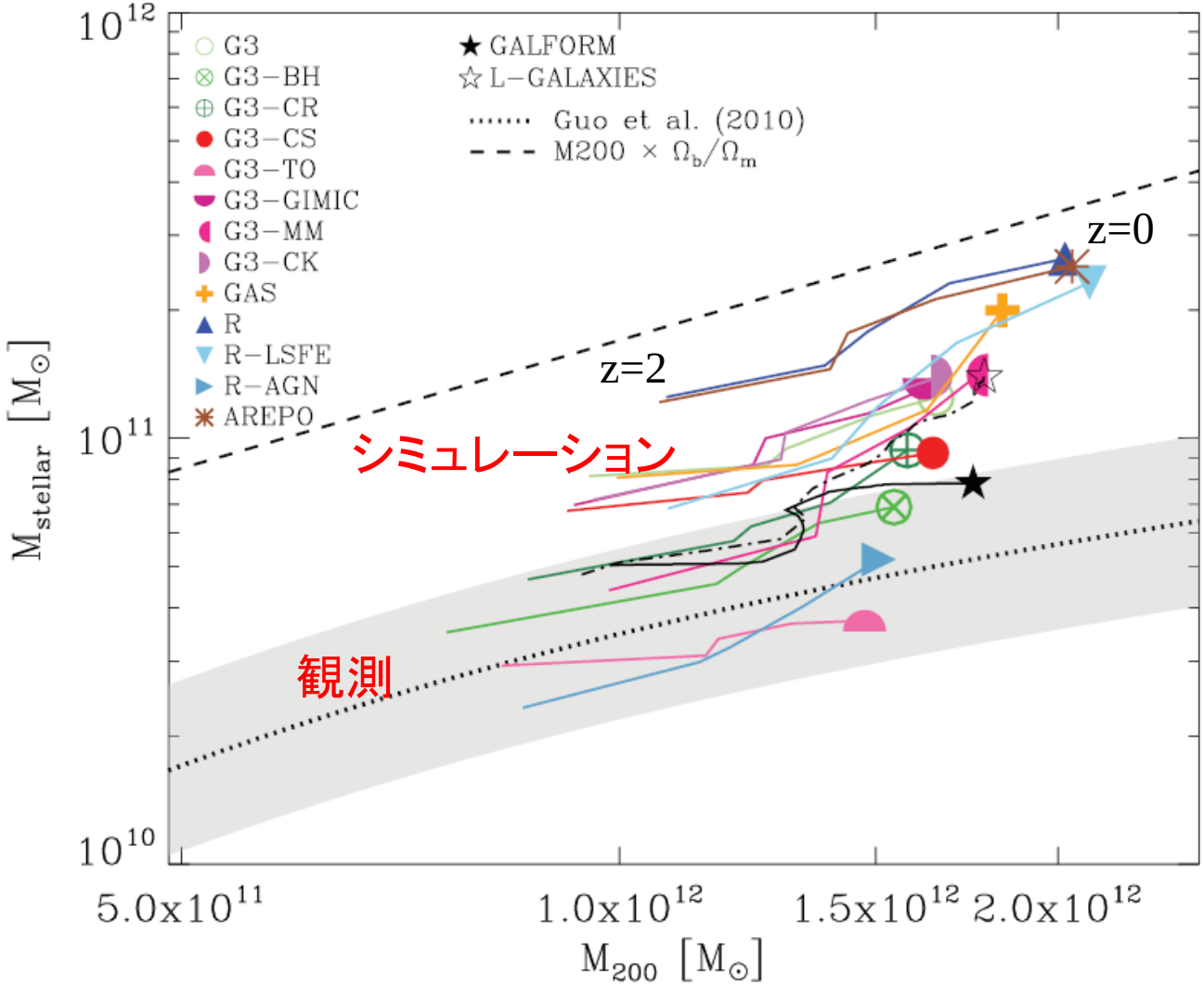

ダークハローの中で星になる割合が観測に比べて多すぎる

Scannapieco et al 2012

角運動量問題

Tully-Fisher 関係

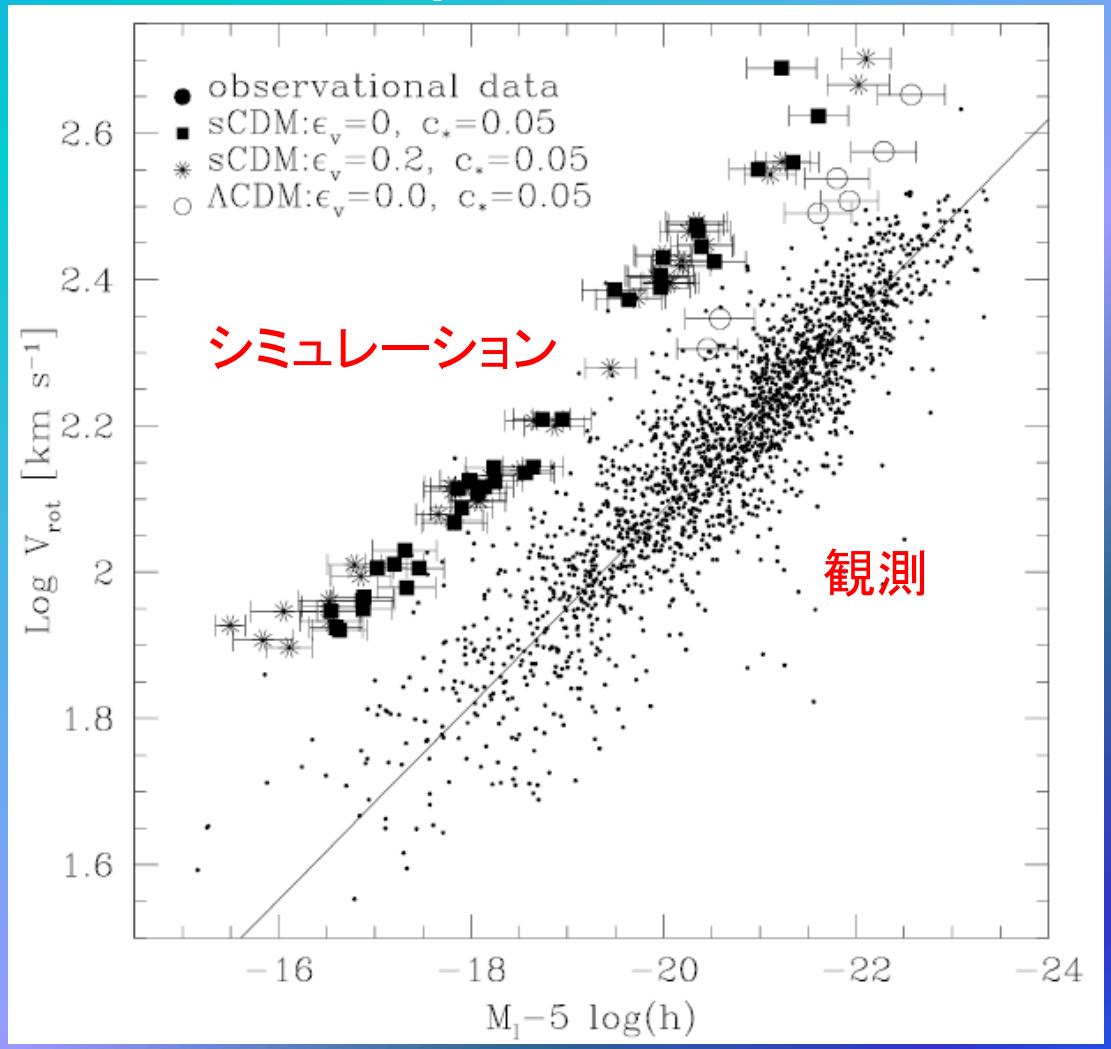

Navarro & Steinmetz 2000

シミュレーション結果は，観測に比べて，システマティックに回転が速い

⇓

重たいバルジが出来すぎる

角運動量問題

Tully-Fisher 関係

The Aquila comparison project

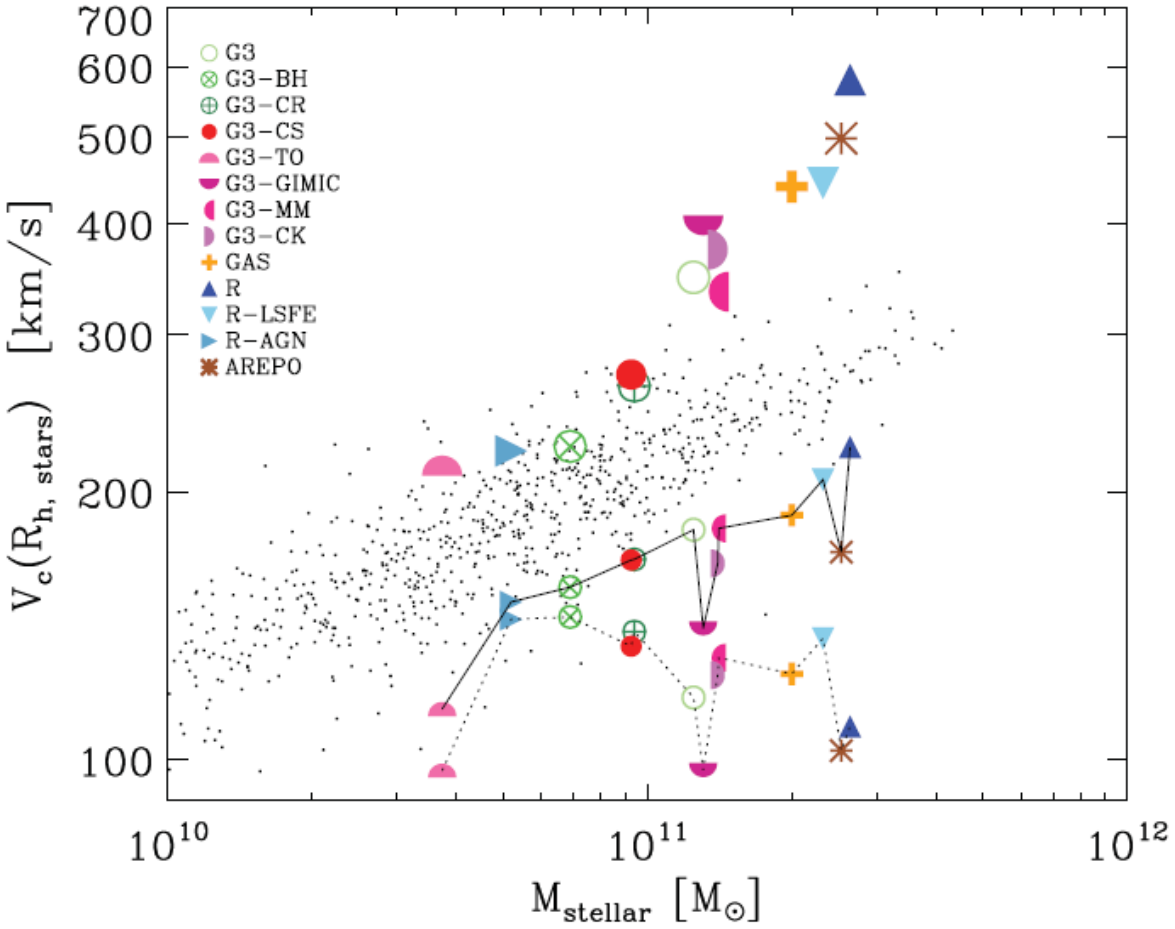

Figure 7. The Tully–Fisher relation. The circular velocity at the stellar half-mass radius of each simulated galaxy is plotted as a function of stellar mass for all 13 level-5 runs. Small black dots correspond to data for nearby spirals taken from Pizagno et al. (2007), Verheijen (2001) and Courteau et al. (2007). The symbols connected by a solid line show the contribution of the dark matter to the circular velocity at $R_{h,stars}$. Those connected by the dotted line show the circular velocity of the dark-matter-only halo (Aq-C) at the same radii.

The origin of discs and spheroids in simulated galaxies

Laura V. Sales,[1★] Julio F. Navarro,[2] Tom Theuns,[3,4] Joop Schaye,[5]
Simon D. M. White,[1] Carlos S. Frenk,[3] Robert A. Crain[5] and Claudio Dalla Vecchia[6]

Mon. Not. R. Astron. Soc. **423,** 1544–1555 (2012)

1) 銀河合体は楕円成分形成にとって重要ではない。楕円成分の星は主にその場で作られたものである。
2) 銀河形態に重要なのは，銀河を作る降着ガスの角運動量の揃い方である。
3) 銀河形態は，初期段階での潮汐場と物質形状との相互作用によって決まる。

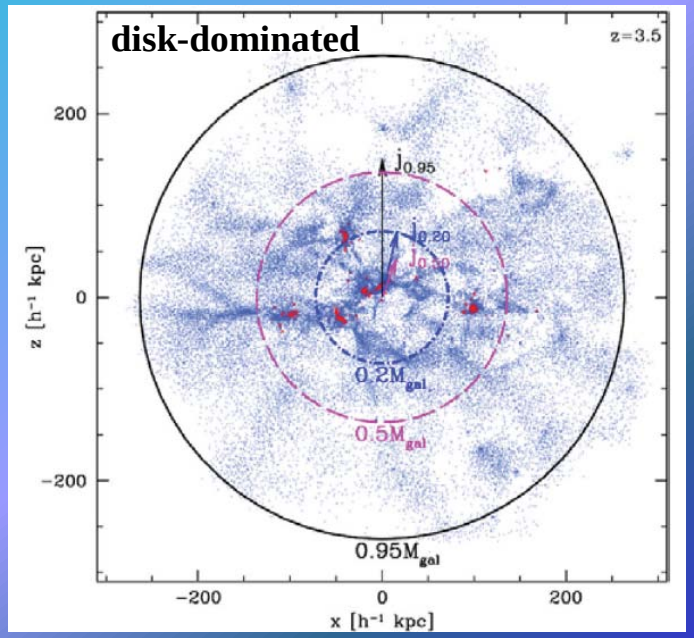

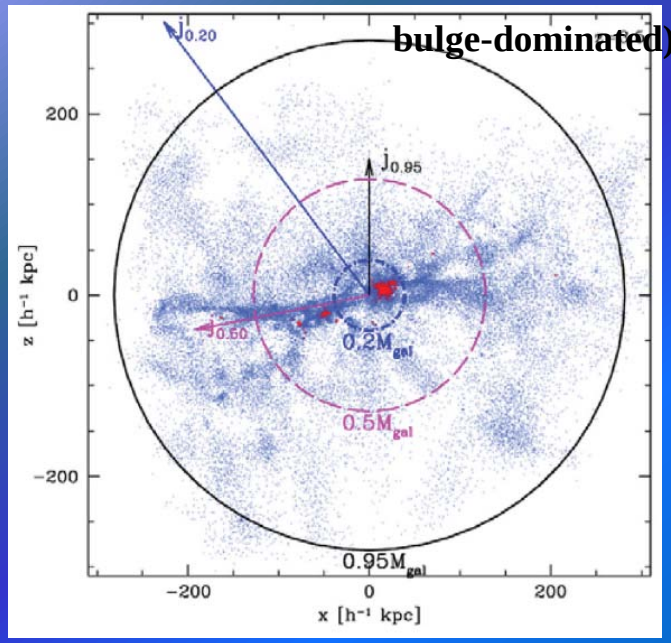

near turn-around time z=3.5

regions of radius ~20 h^{-1} Mpc each are selected from the Millennium Simulation

$$\kappa_{\rm rot} = \frac{K_{\rm rot}}{K} = \frac{1}{K}\sum \frac{1}{2} m \left(\frac{j_z}{R}\right)^2$$

$$\epsilon_j = j_z / j_{\rm circ}(E)$$

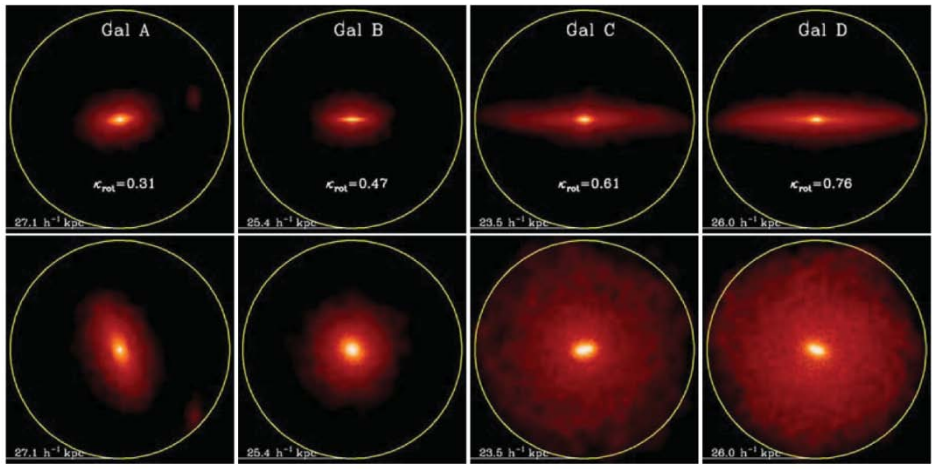

Figure 2. Illustration of the structure of four galaxies in our sample with increasing degree of rotational support (left to right). The first and second rows show edge-on and face-on projections of the stellar distribution. The yellow circle marks the radius, $r_{\rm gal} = 0.15 r_{200}$, used to define the galaxy.

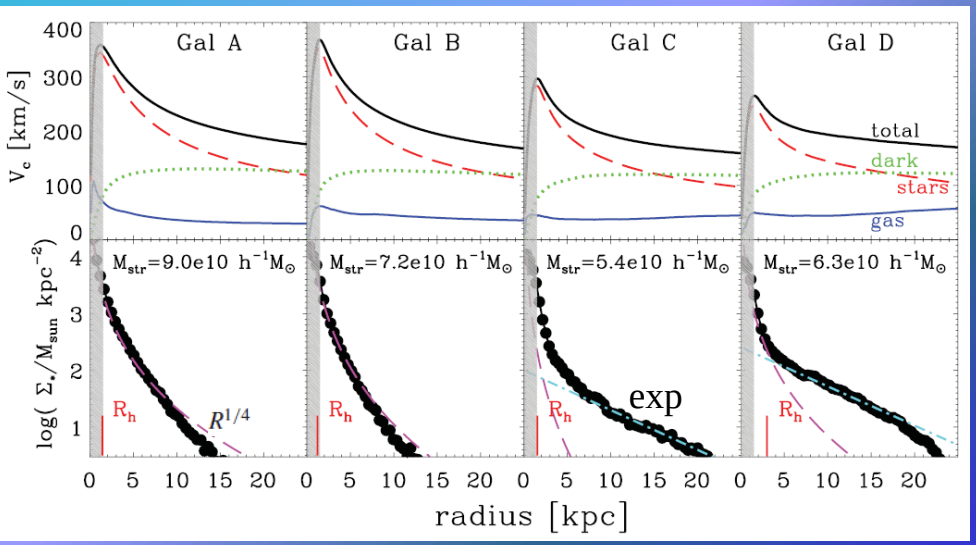

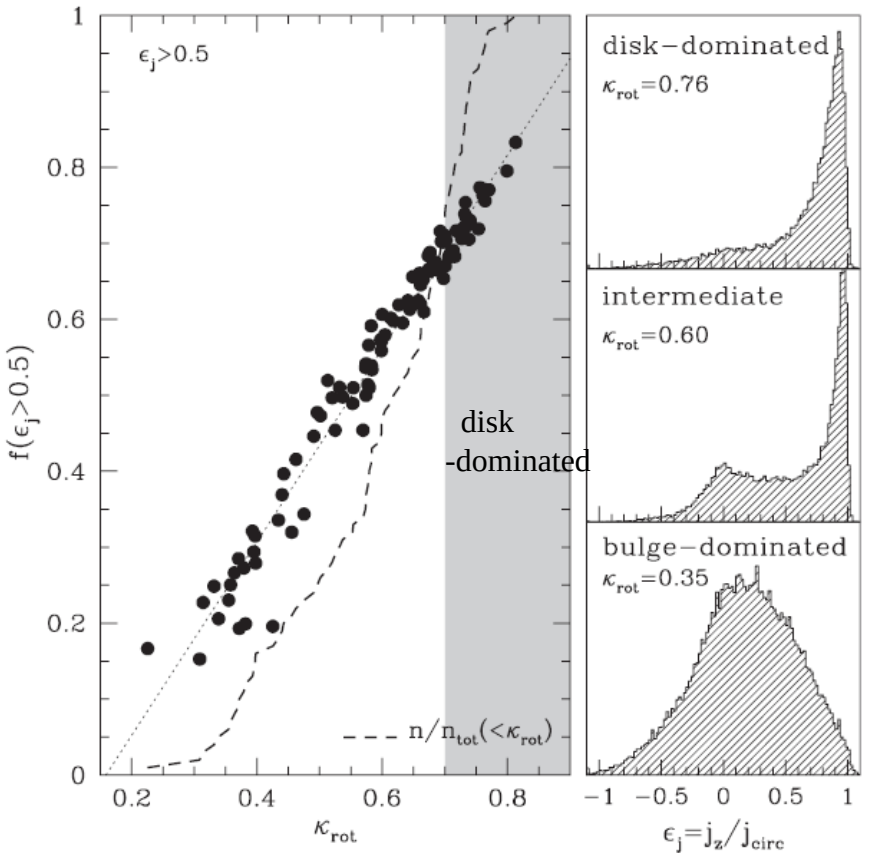

Figure 1. Left: the kinematic morphology parameter, $\kappa_{\rm rot}$, defined as the fraction of kinetic energy in organized rotation (equation 1), versus the fraction of stars with circularity parameter $\epsilon_j > 0.5$. The cumulative fraction is shown with a dashed line. The shaded region ($\kappa_{\rm rot} > 0.7$) indicates where 'disc-dominated' galaxies lie in this plot. Right: the distribution of circularities, $\epsilon_j = j_z/j_{\rm circ}(E)$, is shown for three galaxies with different values of $\kappa_{\rm rot}$.

Observations

Cold gas accretion in galaxies

Sancisi et al. Astron Astrophys Rev, 15, 189 (2008)

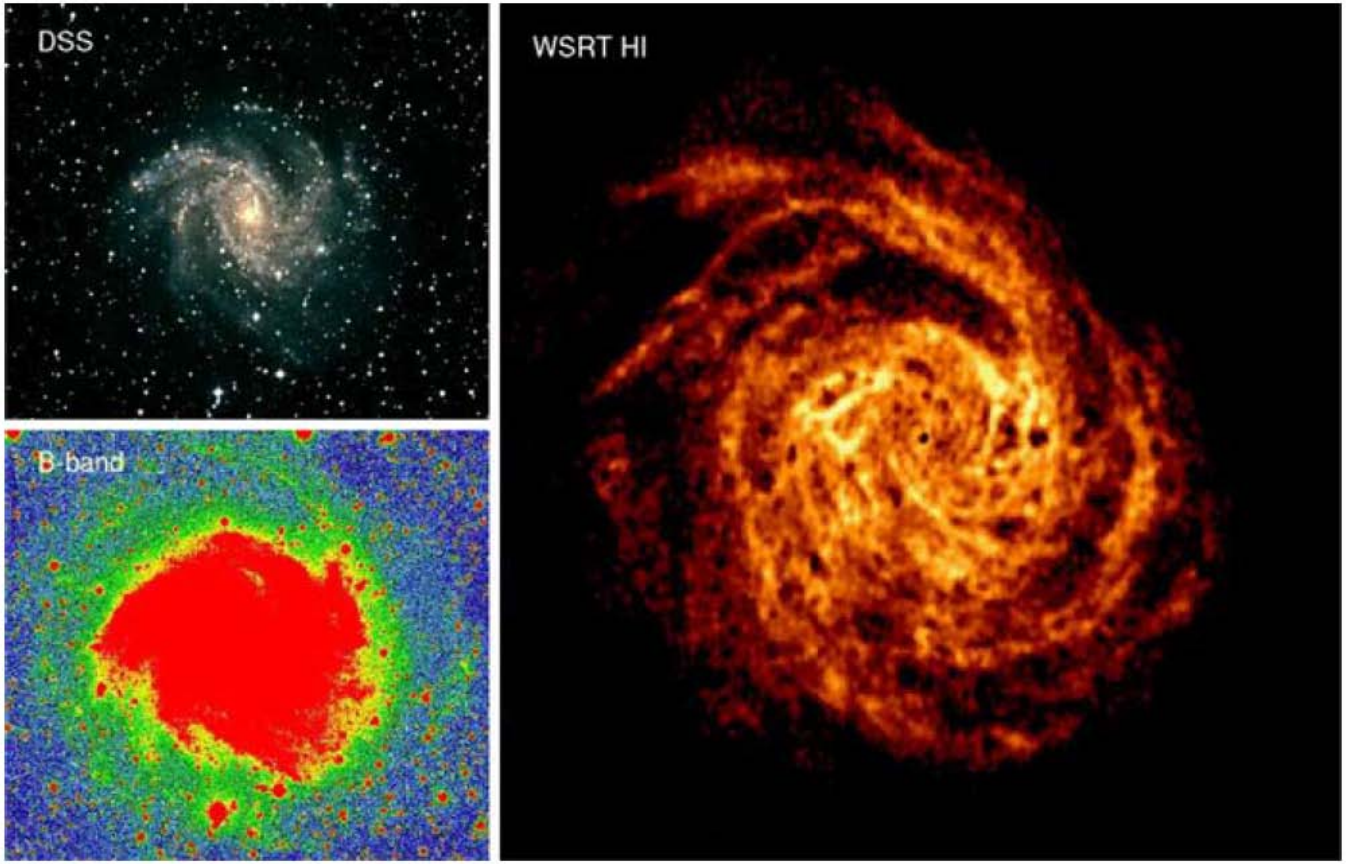

Fig. 10 Comparison between optical images and total H I map for NGC 6946. All images are on the same scale. *Top left* color composite of the Digitized Sky Survey plates. *Bottom left* deep B-band image from Ferguson et al. (1998). *Right* deep WSRT total H I map from Boomsma (2007). Column densities range from 6×10^{19} atoms cm^{-2} to 3×10^{21} atoms cm^{-2}

NGC6946

Stellar spiral の外側に HI gas spiral 構造がある

＋

速度擾乱あり

↓

Infalling clumps of material

Clumpy Galaxies

現在のdisk galaxy のprogenitor は？　thick-disk ×→ thin disk

Clump Clusters

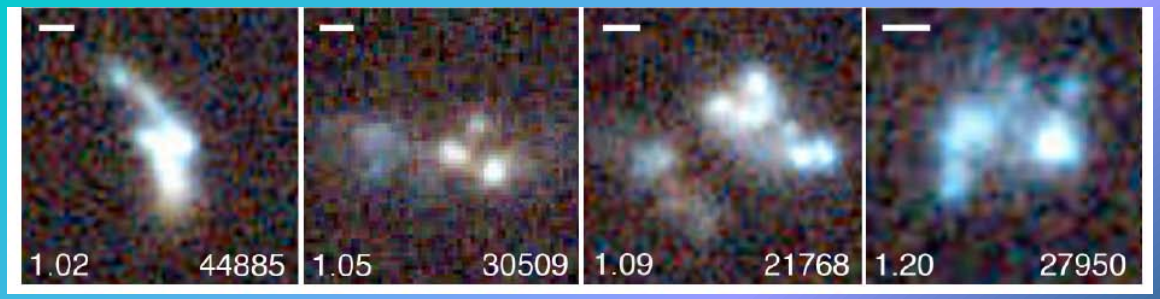

GOODS field

Clumpy Galaxies

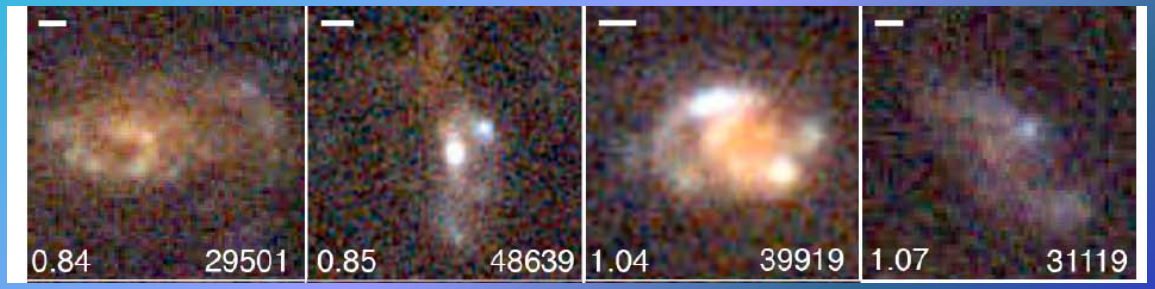

Flocculent Spirals

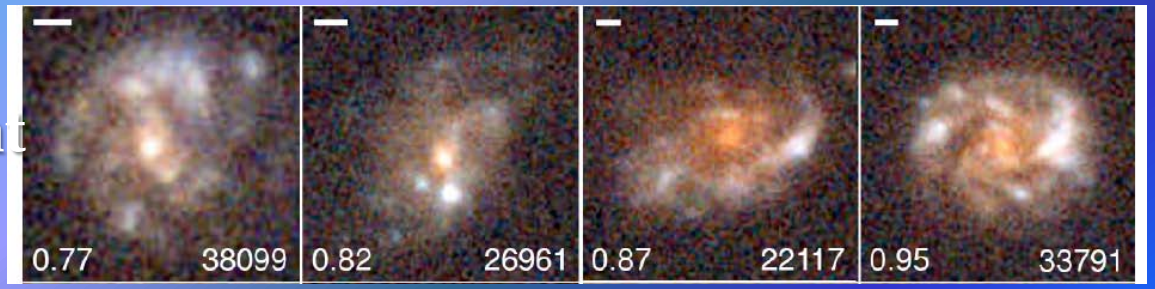

Spirals

Elmegreen et al
701, 306 (2009)

Cold Accretion in Galaxy Formation

1. Galaxy bimodality due to cold flows and shock heating
   Dekel & Birnboim, MNRAS, 368, 2 (2006)

2. Cold streams in early massive hot haloes as the main mode of galaxy formation
   Dekel et al. Nature, 457, 451 (2009)

3. The role of clod flows in the assembly of galaxy disks
   Brooks et al. ApJ, 694, 396 (2009)

4. Modeling the star forming universe at z=2: impact of cold accretion flow
   Khochfar & Silk, ApJL, 700, L21 (2009)

5. High-redshift clumpy discs and bulges in cosmological simulations
   Ceverino, Dekel & Bournaud, MNRAS, 404, 2151 (2010)

6. Moving mesh cosmology: tracing cosmological gas accretion
   Nelson et al. MNRAS 429, 3353 (2013)

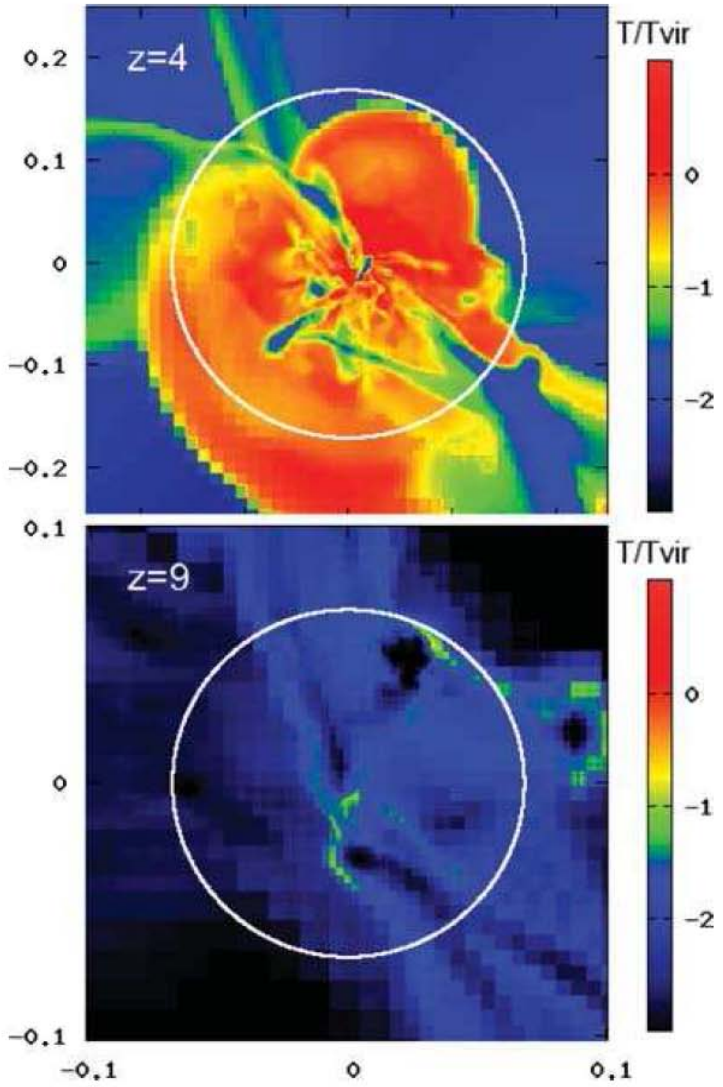

Figure 5. Snapshots from a cosmological hydrodynamical simulation (Birnboim et al. in preparation) showing the gas temperature in a slice of a protogalaxy at two different epochs, when it has two different masses. The temperature is relative to the virial temperature of the halo at that time. The side of each slice is scaled to be $3R_v$ (numbers in comoving h^{-1} Mpc). Top: At $z \simeq 4$, when the halo is already relatively massive, $M \simeq 3 \times 10^{11}\,M_\odot$. Much of the gas is heated by a strong shock near the virial radius (white circle). Cold streams penetrate through the hot medium deep into the halo. Bottom: At $z \simeq 9$, when the halo is still small, $M \simeq 2 \times 10^{10}\,M_\odot$. The gas flows in cold ($T \ll T_v$), showing no evidence for shock heating inside the virial radius (circle).

Dekel & Birnboim, MNRAS, 368, 2 (2006)

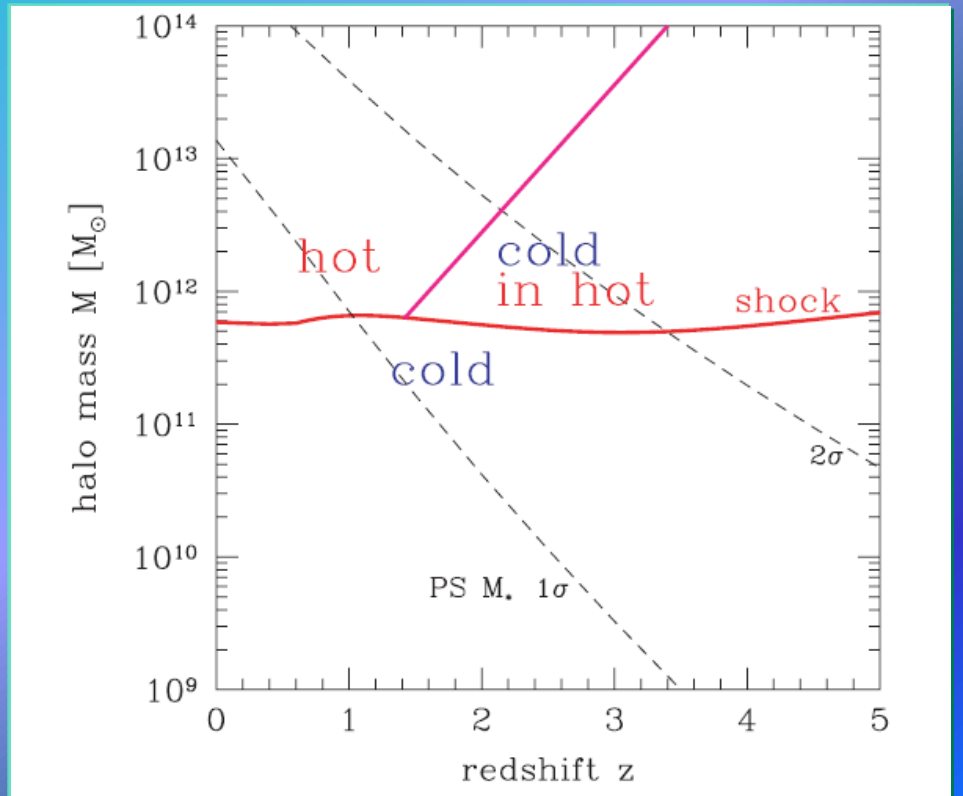

Figure 7. Cold streams and shock-heated medium as a function of halo mass and redshift. The nearly horizontal curve is the typical threshold mass for a stable shock in the spherical infall from Fig. 2, below which the flows are predominantly cold and above which a shock-heated medium is present. The inclined solid curve is the upper limit for cold streams from equation (40) with $f = 3$; this upper limit is valid at redshifts higher than $z_{crit} \sim 1$–2, defined by $M_{shock} > fM_*$. The hot medium in $M > M_{shock}$ haloes at $z > z_{crit}$ hosts cold streams which allow disc growth and star formation, while haloes of a similar mass at $z < z_{crit}$ are all hot, shutting off gas supply and star formation.

Cosmological MareNostrum simulation (adaptive-mesh hydrodynamics)

Dekel et al. 2009, Nature, 457, 451

Star forming galaxies indicate extended, clumpy, thick rotating disks that are incompatible with the expected compact or highly perturbed kinematics of ongoing mergers.
A necessary condition is a steady, rapid gas supply into massive disks.

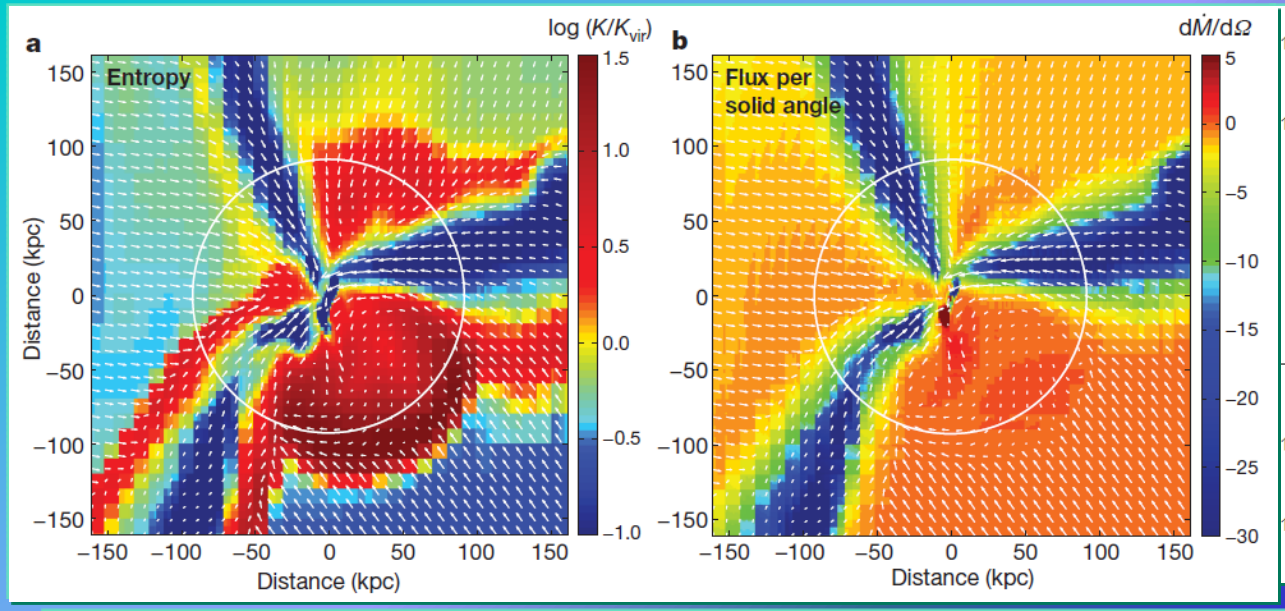

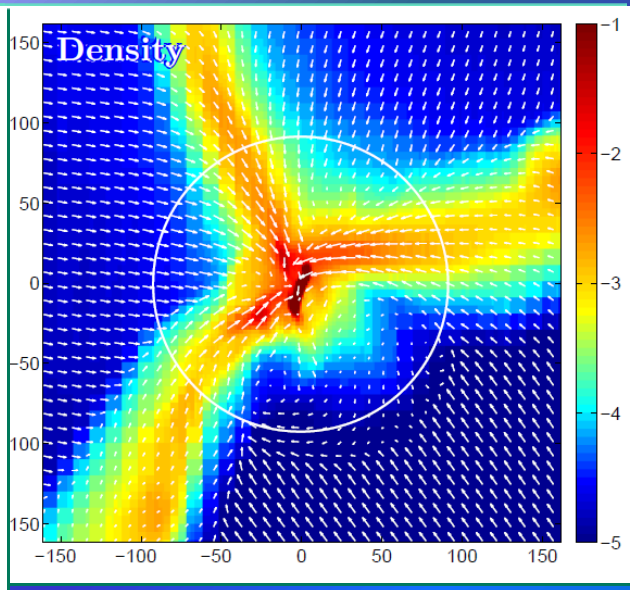

Figure 1 | Entropy, velocity and inward flux of cold streams penetrating hot haloes. **a**, **b**, Maps referring to a thin slice through one of our fiducial galaxies with $M_v = 10^{12} M_\odot$ at $z = 2.5$. The arrows describe the velocity field, scaled such that the distance between the tails is 260 km s^{-1}. The circle marks the halo virial radius, R_v. The entropy, $\log K = \log(T/\rho^{2/3})$, in units of the virial quantities, highlights (in red) the high-entropy medium filling the halo out to the virial shock outside R_v. It exhibits (in blue) three radial, low-entropy streams that penetrate the inner disk, seen edge-on. The radial flux per solid angle is $\dot{m} = r^2 \rho v_r$, in solar masses per year per square radian, where ρ is the gas density and v_r the radial velocity. It demonstrates that more than 90% of the inflow is channelled through the streams (blue), at a rate that remains roughly the same at all radii. This rate is several times higher than the spherical average outside the virial sphere, $\dot{m}_{vir} \approx 8 M_\odot$ yr^{-1} rad^{-2}, according to equation (1). The opening angle of a typical stream at R_v is $20° - 30°$, so the streams cover a total angular area of ~0.4 rad^2, namely a few per cent of the sphere. When viewed from a given direction, the column density of cold gas below 10^5 K is above 10^{20} cm^{-2} for 25% of the area within the virial radius. Although the pictures show the inner disk, the disk width is not resolved, so associated phenomena such as shocks, star formation and feedback are treated in an approximate way only (see density maps and additional cases in Supplementary Figs 3–5). K_{vir}, virial entropy.

SPH vs Moving Mesh

Nelson et al. MNRAS 429, 3353 (2013)

AREPO shows a much lower cold fraction than GADGET, for instance, <20 per cent in haloes with M_{halo}~10^{11}M . .

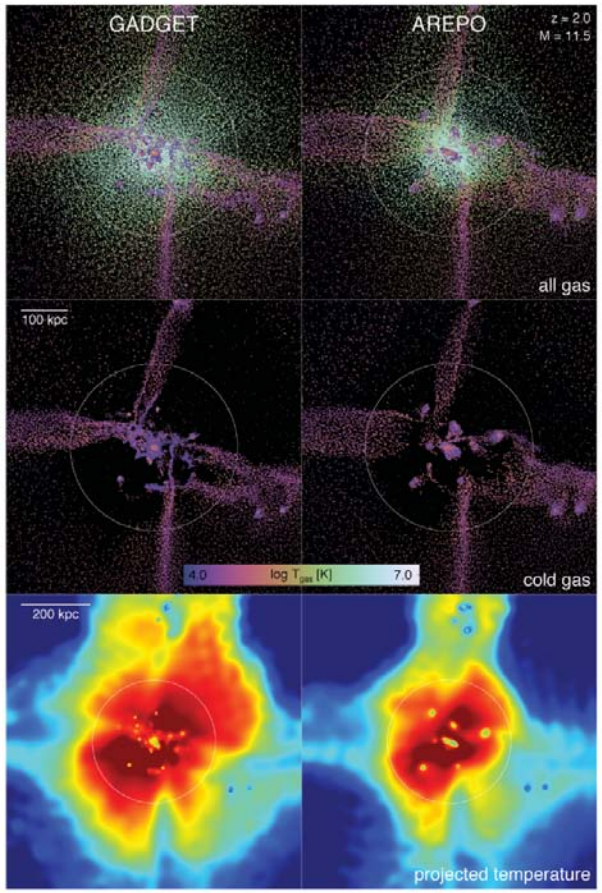

Figure 7. Density and temperature distributions of individual gas elements for an $\simeq 10^{11.5}$ M$_\odot$ halo at $z = 2$ in GADGET (left-hand panels) and AREPO (right-hand panels). The top panels show gas of all temperatures, while the middle panels show only gas with instantaneous temperature $T < 10^5$ K. The ticks are colour coded by instantaneous temperature and with directions representative of the local velocity field. The bottom panels show the mass-weighted temperature projection for lines of sight through a larger cube of side length $5r_{vir}$. The same DM halo in AREPO has a less extended hot component than its GADGET counterpart. In both cases, locally overdense and overcool filamentary gas structures penetrate the hot halo at r_{vir} and deliver gas to smaller radii. In GADGET these filaments become extremely collimated and cold at $\sim 0.5r_{vir}$, whereas in AREPO they tend to become more diffuse, dissipate or experience significant heating. The latter case can be seen at the top of the left-hand filament which shows a thin, $\sim 10^6$ K streamer.

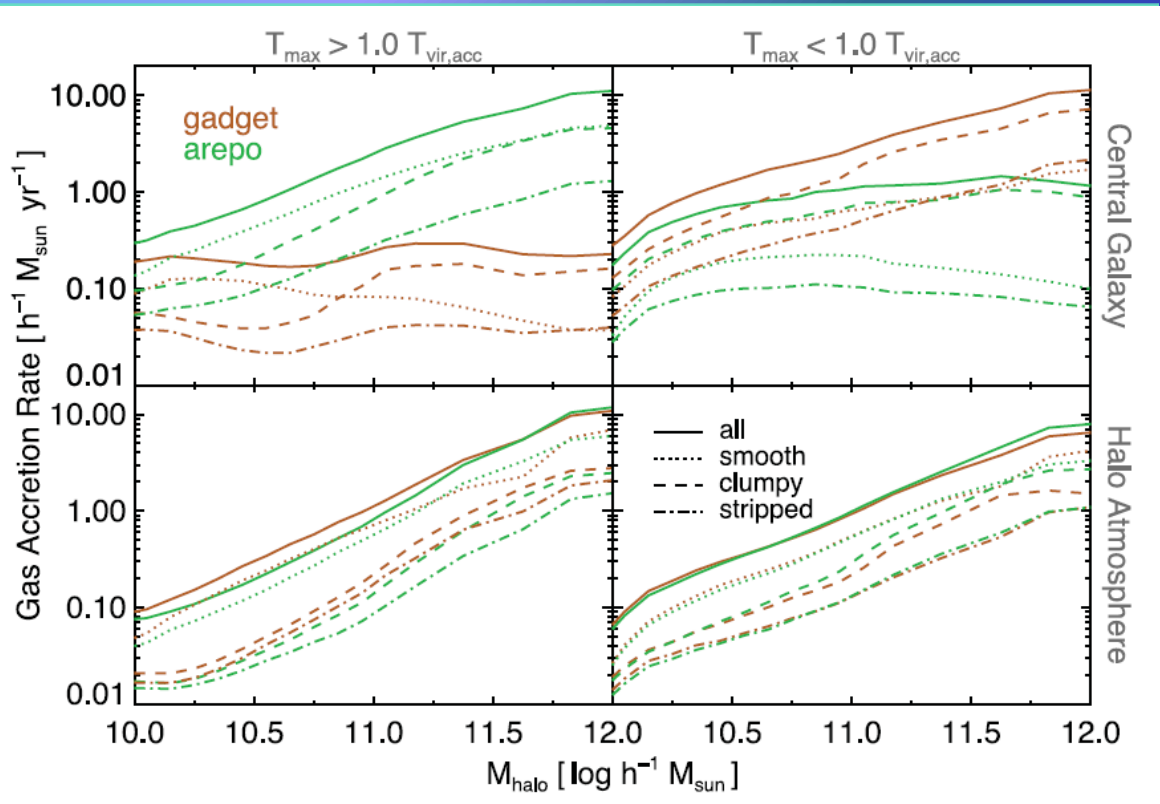

Summary

円盤銀河形成シミュレーションの問題

- 質量問題
- 角運動量問題
- clumpy disk 形成

今後の課題

- Cold accretion w/ star formation
- Accurate thermal processes
- Internal UV Radiation transfer
- UV ≡ SN feedback
- AGN radiative/mechanical feedback